

$i_N$ RACM: Incorporating  $^{15}\text{N}$  into the Regional Atmospheric Chemistry Mechanism (RACM) for assessing the role photochemistry plays in controlling the isotopic composition of  $\text{NO}_x$ ,  $\text{NO}_y$ , and atmospheric nitrate.

Huan Fang. *Purdue University, Department of Earth, Atmospheric, and Planetary Sciences. West Lafayette, IN. USA*

Wendell Walters. *Brown University, Institute for Environment and Society*

David Mase. *Purdue University, Department of Earth, Atmospheric, and Planetary Sciences. West Lafayette, IN. USA*

Greg Michalski. *Purdue University, Department of Earth, Atmospheric, and Planetary Sciences, Department of Chemistry. West Lafayette, IN. USA*

#### Key Points

- Modeling nitrogen isotope fractionation during the photochemical oxidation of nitrogen oxides into atmospheric nitrate.
- Incorporation of N isotopes of  $\text{NO}_y$  into the Regional Atmospheric Chemistry Mechanism.
- Implications for quantifying  $\text{NO}_x$  sources and oxidation pathways using nitrogen isotopes.

## Abstract

Nitrogen oxides, classified as  $\text{NO}_x$  (nitric oxide (NO) + nitrogen dioxide ( $\text{NO}_2$ )) and  $\text{NO}_y$  ( $\text{NO}_x$  +  $\text{NO}_3$ ,  $\text{N}_2\text{O}_5$ ,  $\text{HNO}_3$ , +  $\text{HNO}_4$  + HONO + Peroxyacetyl nitrate (PAN) + organic nitrates + any oxidized N compound), are important trace gases in the troposphere, which play an important role in the formation of ozone, particulate matter (PM), and secondary organic aerosols (SOA). There remain many uncertainties in origin and fate of atmospheric N compounds including the understanding of  $\text{NO}_y$  cycling,  $\text{NO}_x$  emission budgets, unresolved issues within the heterogeneous uptake coefficients of  $\text{N}_2\text{O}_5$ , and the formation of organic nitrates in urban forests, to name a few. A potential tool to resolve some of these uncertainties are using natural abundance N isotopes in  $\text{NO}_y$  compounds. Here we have developed a photochemical mechanism used to simulate tropospheric photochemistry to include  $^{15}\text{N}$  compounds and reactions as a means to simulate  $\delta^{15}\text{N}$  values in  $\text{NO}_y$  compounds. The 16 N compounds and 96 reactions involving N used in Regional Atmospheric Chemistry Mechanism (RACM) were replicated using  $^{15}\text{N}$  in a new mechanism called  $i_{\text{N}}\text{RACM}$ . The 192 N reactions in  $i_{\text{N}}\text{RACM}$  were tested to see if isotope effects were relevant with respect to significantly changing the  $\delta^{15}\text{N}$  values ( $\pm 1\%$ ) of  $\text{NO}_x$ , HONO, and/or  $\text{HNO}_3$ . The isotope fractionation factors ( $\alpha$ ) for relevant reactions were assigned based on recent experimental or calculated values. Each relevant reaction in the  $i_{\text{N}}\text{RACM}$  mechanism was tested individually and in concert in order to assess the controlling reactions. The controlling reactions and their diurnal importance are discussed. A comparison between  $i_{\text{N}}\text{RACM}$  predictions and observed  $\delta^{15}\text{N}$   $\text{NO}_3^-$  in particulate matter from Tucson, AZ. suggests the model, and isotope fractionation factors incorporated into it, are accurately capturing the isotope effects occurring during the photochemistry of  $\text{NO}_y$ . The implication is that measurements of  $\delta^{15}\text{N}$  in  $\text{NO}_y$  compounds may be a new way of tracing *in situ* N chemistry and as a means of assessing  $\text{NO}_x$  emission budgets.

## 1. Introduction

Nitrogen oxides are an integral part of atmospheric chemistry, controlling the oxidation state of the troposphere, influencing aerosol formation, altering the pH of rainwater, and facilitating the movement of nitrogen through the N cycle. Nitrogen oxides are classified as  $\text{NO}_x$  (nitric oxide (NO) + nitrogen dioxide ( $\text{NO}_2$ )) and  $\text{NO}_y$  ( $\text{NO}_x + \text{NO}_3, \text{N}_2\text{O}_5, \text{HNO}_3, + \text{HNO}_4 + \text{HONO} + \text{Peroxyacetyl nitrate (PAN)} + \text{organic nitrates} + \text{any oxidized N compound}$ ) [Day *et al.*, 2003; Hegglin *et al.*, 2006; Ma *et al.*, 2013].  $\text{NO}_x$  produces ozone ( $\text{O}_3$ ) through  $\text{NO}_2$  photolysis, and  $\text{NO}_x$  acts as a catalyst in  $\text{O}_3$  production when volatile organic compounds (VOCs) are present. In turn,  $\text{O}_3$  photolysis generates OH radicals, which initiates a radical chain reaction involving  $\text{HO}_2$  and organic peroxide propagators that result in the oxidation of chemically reduced compounds in the troposphere making them more soluble [Finlayson-Pitts and Pitts, 2000; Seinfeld and Pandis, 1998]. Thus,  $\text{NO}_x$  facilitates the cleansing of the atmosphere through the production of  $\text{O}_3$  and  $\text{OH}_x$  ( $\text{OH} + \text{HO}_2$ ), which together define the troposphere's oxidation state [Bloss *et al.*, 2005; Lelieveld *et al.*, 2008; Prinn, 2003]. These oxidants play an important role in the formation of particulate matter (PM) [Bauer *et al.*, 2007; Pye *et al.*, 2010], forming secondary organic aerosols (SOA) via VOC oxidation [Hoyle *et al.*, 2011; Shrivastava *et al.*, 2017]. They also generate secondary inorganic PM through  $\text{NO}_x$ , sulfur oxides ( $\text{SO}_x$ ), and ammonia ( $\text{NH}_3$ ) neutralization, which leads to ammonium nitrate ( $\text{NH}_4\text{NO}_3$ ) and ammonium sulfate ( $(\text{NH}_4)_2\text{SO}_4$ ) production [Cao *et al.*, 2017; Pan *et al.*, 2018; Pusede *et al.*, 2016]. The production of PM has important consequences for air quality aerosols [Andreae and Crutzen, 1997], human health [Bruningfann and Kaneene, 1993; Hall *et al.*, 1992], and radiative forcing [Charlson *et al.*, 1992; Chen *et al.*, 2007]. Termination reactions in  $\text{NO}_y$  cycling produces  $\text{HNO}_3$  and facilitates the production of sulfuric acid ( $\text{H}_2\text{SO}_4$ ), two strong acids that decrease the pH of rain, known colloquially as acid rain and impact aerosol pH, both of which triggers a number of negative impacts on the environment [Brimblecombe *et al.*, 2007; Lajtha and Jones, 2013]. When  $\text{NO}_y$  is deposited to the surface by wet and dry deposition, it transfers bioavailable N to ecosystems that may be bereft of, or saturated with, bioavailable N. This process can shift the balance of both terrestrial and aquatic ecosystems and impact the goods and services that those ecosystems can normally deliver [Du *et al.*, 2019; E. M. Elliott *et al.*, 2019; Fowler *et al.*, 2013]. Thus, understanding  $\text{NO}_y$  sources and their chemistry is important for an array of scientific disciplines and evaluating their social, economic, and cultural impact on the environment.

Despite this importance, there are numerous knowledge gaps in the understanding of the cycling of  $\text{NO}_y$  in the atmosphere. The  $\text{NO}_x$  emission budget is still poorly constrained. Most emission inventories rely on fixed emission factors for some sources that may, in fact, be variable. For example, power plant  $\text{NO}_x$  emissions are based on assumed efficiency of catalytic converters that may not be accurate [Shrivastava *et al.*, 2005; Felix *et al.*, 2012]. Soil NO emissions are highly dependent on soils moisture, redox conditions, fertilizer application rates, type, and timing making them challenging to constrain [Shepherd, 1991; Galloway *et al.*, 2004; Hudman *et al.*, 2012; Houlton *et al.*, 2013; Pilegaard, 2013]. There are several unresolved issues with the heterogeneous uptake coefficients of  $\text{N}_2\text{O}_5$  [Brown *et al.*, 2001; Brown *et al.*, 2006; Chang *et al.*, 2011] and the formation of organic nitrates in urban forests [Lee *et al.*, 2016; Romer *et al.*, 2016; Kastler and Ballschmiter, 1998]. The relative importance and mechanism of HONO formation versus HONO emissions are also hotly debated. Likewise, reactions of  $\text{NO}_y$  in the aqueous phase and mixed aerosols are not fully understood. Chemical transport models (CTMs) do not accurately predict

aerosol nitrate concentrations or other NO<sub>y</sub> mixing ratios [Spak and Holloway, 2009; Zhang et al., 2009]. Therefore, it is important that these uncertainties in NO<sub>y</sub> cycling be resolved if we aim to have accurate air quality forecast and accurate chemistry-climate models that use CTMs.

It has been suggested that stable N isotopes can provide clues as to the origin of NO<sub>x</sub> [Elliott et al., 2009; Felix and Elliott, 2014; Walters et al., 2015b] and the oxidation pathways that transform in NO<sub>y</sub> [Freyer, 1993; Walters and Michalski, 2015; 2016]. Isotopic measurements of NO<sub>y</sub> compounds show a wide range of δ<sup>15</sup>N values (Eq. (1)), which has been suggested to indicate variability in NO<sub>x</sub> emission sources, chemical processing, and/or a combination of these effects. δ<sup>15</sup>N is defined by the relative difference between the <sup>15</sup>N/<sup>14</sup>N ratio in a NO<sub>y</sub> compound and the ratio in air N<sub>2</sub> (the arbitrary reference compound) and is typically reported in parts per thousand e.g. per mil (‰)

$$\delta^{15}\text{N}_{\text{NO}_y}(\text{‰}) = [({}^{15}\text{NO}_y/{}^{14}\text{NO}_y) / ({}^{15}\text{N}_2/{}^{14}\text{N}_2) - 1] * 1000 \quad \text{Eq. (1)}$$

A number of studies have measured the δ<sup>15</sup>N values of NO<sub>x</sub> collected from NO<sub>x</sub> sources such as power plants [Felix et al., 2012], automobiles [Walters et al., 2015a], biomass burning [Fibiger and Hastings, 2016], and non-road sources [Felix and Elliott, 2014].

Many studies have measured the δ<sup>15</sup>N values of various NO<sub>y</sub> compounds collected from the troposphere. Most of the NO<sub>y</sub> δ<sup>15</sup>N data is for nitrate that has been collected on filters (PM<sub>2.5</sub>, PM<sub>10</sub>, TSP) [Moore, 1977; Savard et al., 2017], as the dissolved NO<sub>3</sub><sup>-</sup> anion in rain [Heaton, 1987; Hastings et al., 2003; Felix et al., 2015; Yu & Elliott, 2017], or as gas phase HNO<sub>3</sub> [Elliott et al., 2009; Savard et al., 2017]. The range of tropospheric NO<sub>y</sub> δ<sup>15</sup>N values span -50 to +15‰ but the average is ~0‰. Two hypotheses have been offered to explain these ranges: Source and Photochemistry. The source hypothesis [Elliott et al., 2007; Hastings et al., 2013] suggesting that the tropospheric NO<sub>y</sub> δ<sup>15</sup>N value range reflects the spatial and temporal mixing of NO<sub>x</sub> sources with different δ<sup>15</sup>N values that is then converted into NO<sub>y</sub>. The photochemistry hypothesis [Freyer, 1991; Freyer et al., 1993; Walters et al., 2018] suggests that the observed NO<sub>y</sub> δ<sup>15</sup>N variations arise via isotope effects occurring when photochemical cycling partitions N into the myriad of NO<sub>y</sub> compounds. These two hypotheses are not mutually exclusive. Indeed, it is likely to be a combination of both processes, but their relative importance likely shifts depending on environmental conditions such as a region's NO<sub>x</sub> source diversity, plume versus dispersed chemistry, photolysis intensity, and oxidant load. In turn, the δ<sup>15</sup>N data might be a new key to reconciling some of the current uncertainties in NO<sub>y</sub> sources and chemistry, if it can be properly interpreted.

What has become clear is that the temporal-spatial heterogeneity of NO<sub>x</sub> sources and the complex photochemistry of NO<sub>y</sub> presents a serious challenge to deciphering the observed NO<sub>y</sub> δ<sup>15</sup>N values. Except for a few isolated cases, a proper assessment of NO<sub>y</sub> δ<sup>15</sup>N values will require incorporating isotope effects into 3-D chemical transport models. This will include emission modeling of <sup>15</sup>NO<sub>x</sub>, meteorological mixing, factoring in isotope effects during NO<sub>y</sub> removal processes, and developing chemical mechanisms that incorporate <sup>15</sup>N compounds and their relative rate constants. Here we take the first step in this endeavor by developing a chemical mechanism (0-D photochemical box model) that explicitly includes <sup>15</sup>NO<sub>y</sub> compounds and the isotope effects that occur during their cycling through photolysis, equilibrium, and kinetic reactions.

## 2. Methods

### 2.1 Chemical and isotopic compounds and reactions included in $i_N$ RACM

The  $i_N$ RACM model incorporates  $^{15}\text{N}$  into the Regional Atmospheric Chemistry Mechanism (RACM) detailed in Stockwell et al. [Stockwell et al., 1997]. RACM is an extension of the chemical mechanism used in the Regional Acid Deposition Model (RADM2) [Stockwell et al., 1990], but with updated inorganic and organic chemistry. There are 17 stable inorganic compounds, 4 inorganic intermediates, 32 stable organic compounds, including 4 biogenic organics, and 24 organic intermediates in the RACM mechanism. The RACM mechanism uses 237 chemical reactions, including 23 photolysis reactions [Atkinson, 1990; Atkinson et al., 1992]. The rate constants, photolysis cross-sections and the quantum yields for the inorganic compounds were taken from [DeMore et al., 1994]. The RACM mechanism aggregates the thousands of VOC in the atmosphere into 16 anthropogenic and 3 biogenic organic compounds. Part of the aggregation criteria is based on the reactivity of a VOC towards the hydroxyl radical ( $\bullet\text{OH}$ ). Full details on how  $\bullet\text{OH}$  reacts with alkanes, alkenes, aromatics, and other VOCs, and the aggregation rationale, can be found in Stockwell et al. (1997). The actinic flux model used in RACM was developed by Madronich (1987) and calculates the wavelength-dependent photon flux as a function of solar zenith angle, which is a function of time (hourly), date, latitude, and longitude. Inputs to the model include temperature, water vapor content, pressure, initial gas mixing ratios and primary pollutant emission rates. Complete details on the RACM mechanism can be found in Stockwell et al. (1997).

Our  $i_N$ RACM (isotope N in RACM) mechanism was generated by adding  $^{15}\text{N}$  isotopologues for the 2 primary ( $\text{NO}$ ,  $\text{NO}_2$ ) and the 14 secondary N pollutants found in the original RACM mechanism (Table S1a). By definition, an isotopologue is a compound with the same chemical formula but a different mass (e.g.  $\text{NO} = 30$  amu and  $^{15}\text{NO} = 31$  amu, with  $\text{N} = ^{14}\text{N}$ ). This is different from isotopomers, which are isotopic isomers, compounds with the same mass but a different structure caused by isotopic substitution (e.g.  $^{15}\text{NNO}_5 = 109$  amu and  $\text{N}^{15}\text{NO}_5 = 109$  amu). Of all the reactive N compounds only  $\text{N}_2\text{O}_5$  has multiple possible  $^{15}\text{N}$  substitutions and 2 isotopologues were defined in the  $i_N$ RACM:  $^{15}\text{NNO}_5$  and  $\text{N}^{15}\text{NO}_5$ . The  $^{15}\text{N}$  compounds are numbered (Table S1a) and subscripted (a, b) in order to maintain a compound numbering scheme that is consistent with that in Stockwell et al. (1997). The non-N compounds found in both RACM and  $i_N$ RACM mechanisms have been excluded from Table S1a for the sake of brevity but can be found in Stockwell et al. (1997). The 16  $^{15}\text{N}$  compounds (Table S1a) were added to the original RACM FORTRAN code provided by Stockwell by using  $Z = ^{15}\text{N}$  (e.g.  $^{15}\text{NO}$  is defined as ZO).

The 96 chemical reactions involving N compounds (Table S2a-f) were inspected and replicated for  $^{15}\text{N}$  based on classification as the reaction being either “N only” or “multiple N” reactions. Single N reactions are those where only one N compound was found in the products and reactants, for example  $\text{NO} + \text{O}_3 \rightarrow \text{NO}_2 + \text{O}_2$ . Multiple N reactions could have multiple N compounds in the reactants, the products, or both. Examples of these possible multiple N reactions are  $\text{NO}_2 + \text{NO}_3 \rightarrow \text{N}_2\text{O}_5$ ,  $\text{N}_2\text{O}_5 \rightarrow \text{NO}_2 + \text{NO}_3$ , and  $\text{NO}_3 + \text{NO} \rightarrow \text{NO}_2 + \text{NO}_2$  respectively. For these multiple N reactions, a reaction probability was factored into the isotopologue/isotopomer rate constants (discussed below). For example, the N isotopologue/isotopomer equivalent of the  $\text{N}_2\text{O}_5 \rightarrow \text{NO}_2 + \text{NO}_3$  reaction has two isotopomer reactions:  $^{15}\text{NNO}_5 \rightarrow ^{15}\text{NO}_2 + \text{NO}_3$  and  $^{15}\text{NNO}_5 \rightarrow \text{NO}_2 + ^{15}\text{NO}_3$ . These two isotopologue rate constants (R54a, R54b) are multiplied by a factor of 1/2 to account for this statistical probability. Similar statistical factors were considered when N

compounds or intermediates decomposed or reacted to form multiple N products (R52a, R52b, R52c, R52d). All N isotopologue reaction stoichiometry is given in Table S2a-f.

## 2.2 Isotope effects included in $i_N$ RACM

The main challenge for developing realistic isotopologue chemistry in  $i_N$ RACM is quantifying the differences in rate constants caused by isotopic substitution. These isotope effects can be classified into four general types: Equilibrium isotope effects (EIE), kinetic isotope effects (KIE), photo-induced isotope fractionation effects (PHIFE), and vapor pressure isotope effects (VPIE). For this study, the most up-to-date isotope fractionations were used when establishing the framework for modeling their effect associated with  $\text{NO}_x$  oxidation chemistry. The established framework will easily enable an adjustment of isotope effects as we improve our understanding of isotope fractionation factors.

Urey (1947) and Bigeleisen and Mayer (1947) showed that EIEs are driven by the sensitivity of molecular and condensed-phase vibrational frequencies to isotopic substitutions [Bigeleisen and Mayer, 1947; Urey, 1947]. Because vibrations are used in the molecular partition function (Q) to calculate equilibrium constants, isotopic substitution results in isotopologues having different equilibrium constants. Urey [1947] defined the reduced partition function ratio for two isotopologues of the same compound as a  $\beta$  value. For example, the reduced partition function ratio of nitric oxide N isotopologues is  $Q_{^{15}\text{NO}}/Q_{\text{NO}} = \beta_{\text{NO}}$ , with the heavy isotope placed in the numerator by convention. The ratio of two  $\beta$  values is denoted as  $\alpha_{\beta_1/\beta_2}$  the isotope fractionation factor. For example,  $\alpha_{\text{NO}/\text{NO}_2}$  is the temperature-dependent isotope fractionation factor (EIE) for the  $\text{NO} + ^{15}\text{NO}_2 \leftrightarrow ^{15}\text{NO} + \text{NO}_2$ . In this case, at 298K  $\beta_{\text{NO}} = 1.0669$  and  $\beta_{\text{NO}_2} = 1.1064$  and  $\alpha_{\text{NO}/\text{NO}_2} = \beta_{\text{NO}}/\beta_{\text{NO}_2} = 0.9643$  [Walters and Michalski, 2015].

A KIE is the relative change in the rate of a unidirectional chemical reaction when one of the atoms of the reactants is substituted with an isotope [Bigeleisen and Wolfsberg, 1958]. KIEs are driven by the change in energy required to proceed over the reaction barrier (transition state) as well as changes in the probability of quantum mechanical tunneling [Wolfsberg et al., 2010]. This generally results in a lighter isotopologue reacting faster than a heavier isotopologue. Much of the early research on KIEs were investigations of the KIE in reactions containing hydrogen isotopes and these studies usually defined a  $\text{KIE} = k_L/k_H = \alpha_{L/H}$ , where the  $k$ 's are the rate constants for the light and heavy isotopologues. This is the inverse of the definition of  $\alpha$  usually used in research dealing with EIE, VPIE, PHIFE and this inversion can lead to confusion. In this paper, in order to maintain consistency between the  $\alpha$  values for EIE, KIE, VPIE, and PHIFE,  $\alpha$  will be defined as heavy/light for all four effects.

The  $\alpha$  values for EIE and KIE can be determined using a number of approaches. The  $\alpha$  values for EIE can be calculated if molecular constants (e.g. harmonic frequencies and anharmonicity constants) of the isotopologue pair are known. Accurate molecular constants are difficult to accurately measure for large molecules and as a result, they primarily exist only for diatomic and triatomic isotopologues [Richet et al., 1977]. The only experimental EIE values for  $^{15}\text{N}$  isotopologues of  $\text{NO}_y$  is for the EIE between  $\text{NO}$  and  $\text{NO}_2$  [Sharma et al., 1970; Walters et al., 2016]. To determine the EIE in other  $\text{NO}_y$  compounds we must rely on quantum chemistry computation methods to estimate the molecular constants and anharmonicity constants. Recent works utilizing these methods have estimated the EIE for most non-organic  $\text{NO}_y$  compounds [Walters and Michalski, 2015]. For KIE, in addition to molecular constants, the transition state

vibrational frequencies are also needed. The only  $^{15}\text{N}$  KIE calculation to date for an  $\text{NO}_y$  compound is for the KIE for the  $\text{NO} + \text{O}_3$  reaction [Walters and Michalski, 2016].

These EIE and KIE values have been incorporated in  $i_{\text{N}}\text{RACM}$  in this study Table S2a-c. If there is no isotope effect associated with any of the  $\text{NO}_y$  reactions, then  $\alpha$  is set equal to 1. The  $^{15}\text{N}$  isotopologue rate constant for any reaction is then  $\alpha^{14}k$  where  $^{14}k$  is the rate constant for any  $^{14}\text{N}$  reaction in RACM and these are given in Table S2a-f. It is useful to define the magnitude of EIE and KIE in the same per mil (‰) notation used to quantify a  $\delta^{15}\text{N}$  values by defining an enrichment factor  $\varepsilon(\text{‰}) = (\alpha - 1)1000$ . For example, the  $\text{NO}_x$  isotope exchange equilibrium mentioned above, the  $\varepsilon_{\text{NO}/\text{NO}_2} = -35.7\text{‰}$ . This means that  $^{15}\text{NO}/\text{NO}$  ratio would be 35.7‰ smaller than the  $^{15}\text{NO}_2/\text{NO}_2$  ratio if the isotopes in two gases were equilibrated (Table S2b).

PHIFE is the relative change in photolysis rates of isotopologues due to the substitution of a heavier isotope [Yung and Miller, 1997]. In the atmospheric N cycle,  $\text{NO}_2$ ,  $\text{NO}_3$ ,  $\text{N}_2\text{O}_5$ , and HONO readily undergo photolysis at wavelengths of light that penetrate into the troposphere. The PHIFE can be estimated using a simple zero-point energy shift model ( $\Delta\text{ZPE}$ ). In this approximation, the absorption spectra of the heavier isotopologue is generated by applying a uniform blue shift (equal to  $\Delta\text{ZPE}$ ) to the measured spectral absorbance of the light (major) isotopologue [Blake et al., 2003; Liang et al., 2004; Miller and Yung, 2000]. This results in isotopic fractionation because the wavelength ( $\lambda$ ) dependent photolysis rate constant ( $J(\lambda)$ ) is dependent on the convolution of the absorption cross-section ( $\sigma(\lambda)$ ), actinic flux ( $F(\lambda)$ ), and quantum yield ( $\phi(\lambda)$ ) (Eq. (2)):

$${}^xJ(\lambda) = {}^x\sigma(\lambda)F(\lambda)\phi(\lambda) \quad \text{Eq. (2)}$$

The overall photolysis rate constant ( ${}^zJ$ ) can be calculated by integrating  $\sigma$ ,  $F$ , and  $\phi$  over a range of wavelengths that can cause dissociation ( $\lambda_1$  and  $\lambda_2$ ):

$${}^zJ = \int_{\lambda_1}^{\lambda_2} {}^x\sigma(\lambda)F(\lambda)\phi(\lambda)d\lambda \quad \text{Eq. (3)}$$

The N isotopologue fractionation ( $\alpha$ ) resulting from photolysis (of  $\text{NO}_2$  isotopologues) is calculated by (Eq. (4)).

$$\alpha_{47/46} = \frac{{}^{47}J}{{}^{46}J} \quad \text{Eq. (4)}$$

It is important to note that there are limitations in the  $\Delta\text{ZPE}$ -shift model [Blake et al., 2003; Liang et al., 2004; Miller and Yung, 2000]. These include the failure to account for changes in shape and intensity of absorption spectra upon isotopic substitution and the same quantum yield (as a function of wavelength) is assumed for all isotopologues. Despite these limitations, this approach should still give a rough estimate of photolytic fractionation until experimentally determined PHIFE's become available [Blake et al., 2003; Liang et al., 2004; Miller and Yung, 2000].

Isotopologues partition differently between phases giving rise to the VPIE. This is most notable in gas-liquid systems [Van Hook et al., 2001], but also can occur in gas-solid equilibrium. Both of these may ultimately be important for understanding  $\delta^{15}\text{N}$  variability in  $\text{NO}_y$  compounds. For example, solid-gas VPIE may be relevant for the  $\text{HNO}_{3(\text{g})} + \text{NH}_{3(\text{g})} \leftrightarrow \text{NH}_4\text{NO}_{3(\text{s})}$  reaction, whose temperature-dependent equilibrium can shift dramatically diurnally [Morino et al., 2006] and seasonally [Paulot et al., 2016]. It is likely that this VPIE will result in the particle phase  $\text{NO}_3^-$

having a different  $\delta^{15}\text{N}$  value compared to the gas phase  $\text{HNO}_3$  [Heaton, 1987]. Additionally, possible VPIE occurring during wet and dry deposition, such as  $\text{HNO}_{3(\text{g})} \rightarrow \text{HNO}_{3(\text{aq})}$  may be relevant for  $\delta^{15}\text{N}$  variations  $\text{NO}_3^-$  in precipitation [Freyer et al., 1993]. Multiphase reactions are not included in RACM since it is only concerned with gas phase reactions. These effects may be important for accurate  $\delta^{15}\text{N}$  predictions and should be addressed in more complex models, but this is a limitation in any “gas phase only” photochemical box model. Similarly,  $\text{NO}_y$  aqueous phase reactions, such as  $2\text{NO}_2 + \text{H}_2\text{O} \rightarrow \text{HNO}_3 + \text{HNO}_2$ , are not included in RACM, which may limit  $i_{\text{N}}\text{RACM}$ 's ability to accurately predict the  $\delta^{15}\text{N}$  values of dissolved  $\text{NO}_3^-$  in rainfall samples.

### 2.3 Sensitivity analysis: Determining the “reaction relevance” of $\text{NO}_y$ isotopologues

The objective of the  $i_{\text{N}}\text{RACM}$  model is to make predictions about the temporal and spatial variation of  $\delta^{15}\text{N}$  value in various N compounds caused by EIE, KIE, and PHIFE, and compare them to observations. Currently, the  $\delta^{15}\text{N}$  observations are largely limited to  $\text{HNO}_3$ , as either particulate or dissolved  $\text{NO}_3^-$ , but there are a few recent measurements of the  $\delta^{15}\text{N}$  values of  $\text{NO}_x$  [Walters et al., 2018] and HONO [Chai and Hastings, 2018]. The  $\delta^{15}\text{N}$  values of organic nitrates and PAN may be made in the not so distant future, but there is no published data to date. Thus, a given isotopologue reaction pair in  $i_{\text{N}}\text{RACM}$  was considered “relevant” if it significantly changed the  $\delta^{15}\text{N}$  value ( $\pm 1\%$ ) of  $\text{NO}_x$ , HONO, or  $\text{HNO}_3$ . This relevance was determined by conducting a sensitivity analysis on the PHIFE, KIE, and EIE effects for all N reactions. This was done by arbitrarily setting  $\alpha = 0.98$  ( $\epsilon = -20\%$ ) for one isotopologue reaction and  $\alpha = 1.0$  for all others, then running a test case. This test case is a 5-day simulation, beginning at 3 AM on March 1 (2007) and simulates mid-latitude suburban chemistry using the trace gas and meteorology parameters given in Table S3a-b. This simulation was repeated 96 times until every N containing reaction was tested. For example,  $\text{NO}_x$ , HONO, or  $\text{HNO}_3$   $\delta^{15}\text{N}$  values are not sensitive to R51 (Fig. 1). The following section discusses which  $i_{\text{N}}\text{RACM}$  reactions are relevant and the approaches used to determine the appropriate  $\alpha$  values for those reactions. These simulations were also used to test whether  $i_{\text{N}}\text{RACM}$  achieve N isotope mass balance via  $\Sigma^{15}\text{N}/\Sigma^{14}\text{N}$  where the sums are the ending abundances of all N compounds. This resulted in  $\delta^{15}\text{N} = 0$  for all simulations. We also tested whether the addition of  $^{15}\text{N}$  isotopologues had any effect on the RACM's predictions of trace gases over time. Plots of mixing ratios of trace gases such as  $\text{HNO}_3$  and  $\text{O}_3$  predicted by RACM versus those  $i_{\text{N}}\text{RACM}$  run under the same conditions (see Stockwell's 24 simulation tests) yield a slope of 1 with an  $R^2 > 0.99$ , which is expected since the addition of  $^{15}\text{N}$  compounds is only about 0.3 % of total  $\text{NO}_x$  and thus should not differ from the RACM predictions.

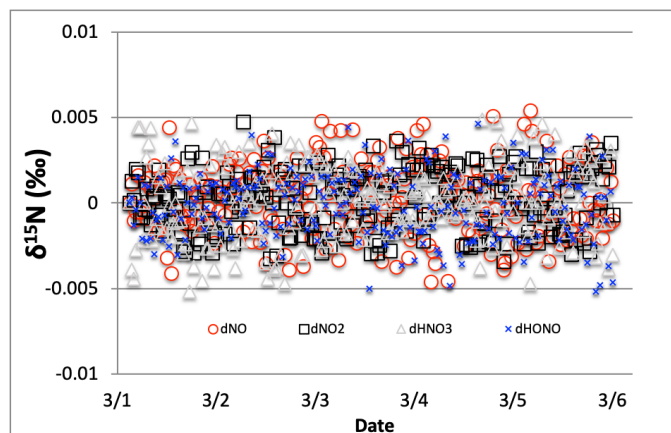


Figure 1. The time evolution of  $\delta^{15}\text{N}$  values of  $\text{NO}$ ,  $\text{NO}_2$ , HONO, and  $\text{HNO}_3$ , caused by the  $\text{NO}_3 + \text{NO} \rightarrow \text{NO}_2 + \text{NO}_2$  reaction (R 51, 51<sub>a</sub>). This reaction only induces a  $\delta^{15}\text{N}$  variation of  $\pm 0.005\%$  in the relevant compounds. Thus, this reaction is considered irrelevant and  $i_{\text{N}}\text{RACM}$  sets R51a  $\alpha = 1.0$ .



### 2.3.1 PHIFE relevant in the $i_N$ RACM mechanism

Only one of the 6 photolysis reactions involving N compounds was found to be relevant.  $\text{NO}_2$  photolysis (R1) had a significant impact on the  $\delta^{15}\text{N}$  value of  $\text{NO}_x$ , HONO, and  $\text{HNO}_3$  (Fig. 2). The initial difference between the  $\delta^{15}\text{N}$  of  $\text{NO}$  and  $\text{NO}_2$  values is roughly equal to the arbitrarily set -20‰ enrichment factor. The nature of the diurnal oscillation in  $\delta^{15}\text{N}$  values on the three relevant  $\text{NO}_y$  compounds and the dampening effect over time will be discussed in the results section.

When there is sufficient photolysis of any single  $\text{NO}_y$  compound, then the  $\delta^{15}\text{N}$  value of that compound tends to significantly change, but often neither the  $\text{HNO}_3$ , HONO, nor  $\text{NO}_x$   $\delta^{15}\text{N}$  values are affected. For example, the arbitrary  $\alpha$  for  $\text{NO}_3$  photolysis (R7 and R8) alters the  $\delta^{15}\text{N}$  value of  $\text{HNO}_3$  and  $\text{NO}_x$  by less than 0.1‰ (not shown), but it induces large diurnal changes in the  $\delta^{15}\text{N}$  value of  $\text{NO}_3$  and  $\text{N}_2\text{O}_5$ , with sharp transitions occurring during sunrise and sunset (Fig. 3). This is easily understood. For our test case, during the day  $^{15}\text{NO}_3$  would be left behind because  $^{14}\text{NO}_3$  is preferentially being photolyzed. The daytime  $\text{N}_2\text{O}_5$  formed from this  $\text{NO}_3$  (positive  $\delta^{15}\text{N}$ ) and  $\text{NO}_2$  ( $\delta^{15}\text{N} \sim 0$ ) thus has a  $\delta^{15}\text{N}$  values halfway between these two reactants (isotope mass balance). However, there is so little  $\text{NO}_3$  and  $\text{N}_2\text{O}_5$  during the day that essentially no  $\text{HNO}_3$  is being formed through these precursors and the  $\text{NO}_3$  PHIFE is not manifested in the  $\text{NO}_x$  or  $\text{HNO}_3$   $\delta^{15}\text{N}$  value. During the night, photolysis and the PHIFE ceases and any  $\text{NO}_3$  and  $\text{N}_2\text{O}_5$  formed by  $\text{NO}_2$  oxidation have  $\delta^{15}\text{N}$  values equal to the  $\text{NO}_2$ .

$\text{NO}_x$ , HONO, and  $\text{HNO}_3$  are not sensitive to the other  $\text{NO}_y$  photolysis reactions because of this isotope mass balance effect.

$$\delta^{15}\text{N}_{\text{NO}_y} = \sum f_{\text{NO}_{yi}} \cdot \delta^{15}\text{N}_{\text{NO}_{yi}} \quad \text{Eq. (5)}$$

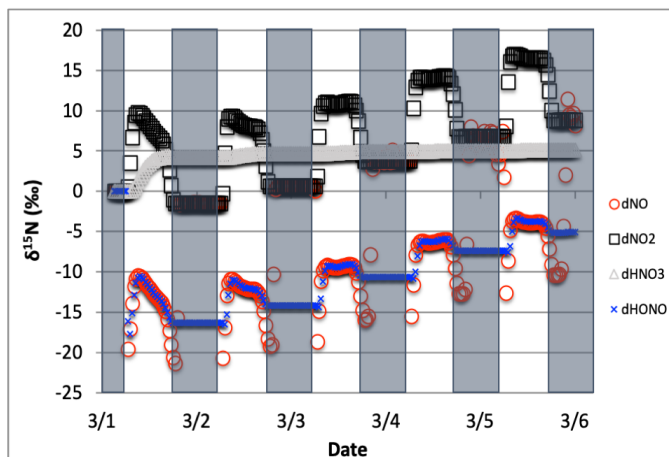


Figure 2. The time evolution of  $\delta^{15}\text{N}$  values of  $\text{NO}$ ,  $\text{NO}_2$ ,  $\text{HNO}_3$ , and HONO caused by PHIFE during  $\text{NO}_2$  photolysis.

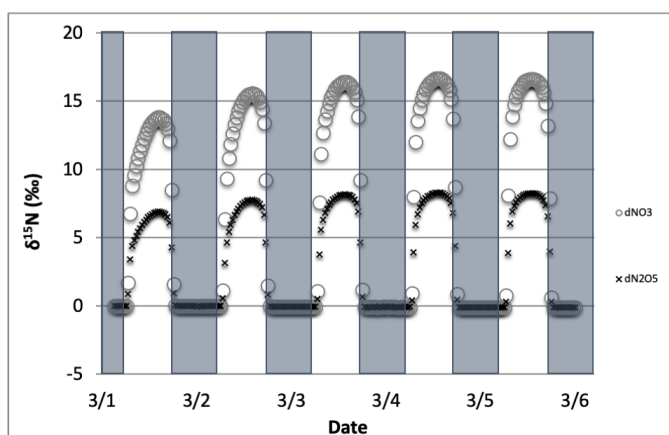


Figure 3. The time evolution of  $\delta^{15}\text{N}$  values of  $\text{NO}_3$ , and  $\text{N}_2\text{O}_5$  caused by PHIFE during  $\text{NO}_3$  photolysis.

Where  $f_{\text{NO}_y}$  is the mole fraction of any  $\text{NO}_y$  compound relative to total  $\text{NO}_y$ ,  $\delta^{15}\text{N}_{\text{NO}_y}$  is the  $\delta^{15}\text{N}$  value of that compound, and  $\delta^{15}\text{N}_{\text{NO}_y}$  is the value of total N, which in these simulations is arbitrarily set to 0‰. For an  $\epsilon = -20\text{‰}$  and a threshold of “importance” set to  $\pm 1\text{‰}$ , isotope mass balance requires that  $f_{\text{NO}_y} > 0.05$ . Only  $\text{NO}$ ,  $\text{NO}_2$ ,  $\text{HONO}$ , and  $\text{HNO}_3$  compounds meet this threshold (Fig. 4). All other  $f_{\text{NO}_y}$  values are an order of magnitude smaller, the largest being  $f_{\text{HNO}_4}$  and it only reaches a maximum value of 0.005. By the end of the second simulation day the  $f_{\text{HNO}_3}$  has approached 1 and effectively minimizes the other  $f_{\text{NO}_y}$  values because it is the only stable N compound because the other  $\text{NO}_y$  compounds are very photochemically active. If we exclude this build up in  $\text{HNO}_3$  from the sum of  $\text{NO}_y$ , then  $f_{\text{NO}}$ , and  $f_{\text{NO}_2}$  (and  $\text{HONO}$  during some hours, see discussion) become the dominant fractions (Fig. 4) and they control the other  $f_{\text{NO}_y}$ . Even under this constraint, the  $f_{\text{HNO}_4}$  only reaches 0.001 (Fig. 4). Thus, in  $i_{\text{NRACM}}$ , the  $\alpha$  values of  $\alpha_{\text{R}4}$ -  $\alpha_{\text{R}8}$  were set equal to 1 and only the  $\alpha_{\text{R}1}$  was assigned a non-1 value, which was determined using a PHIFE theory (discussed below).

### 2.3.2 KIE relevant in $i_{\text{NRACM}}$ mechanism

The KIE for 12 N containing compounds and their 96 reactions were evaluated using the same sensitivity analysis. The vast majority of reactions had little influence on the  $\delta^{15}\text{N}$  values of  $\text{NO}_x$ ,  $\text{HONO}$ , and  $\text{HNO}_3$  (Fig. 1).

Similar to the photolysis sensitivity, either reaction proximity or isotope mass balance were controlling  $\delta^{15}\text{N}$  relevance. For example,  $\text{NO}_2 + \text{OH}$  is reaction that directly produces a significant fraction of  $\text{HNO}_3$  and therefore R39 is relevant in the  $i_{\text{NRACM}}$  mechanism. In contrast, R95 produces very little  $\text{HNO}_3$  so it has a negligible influence on the

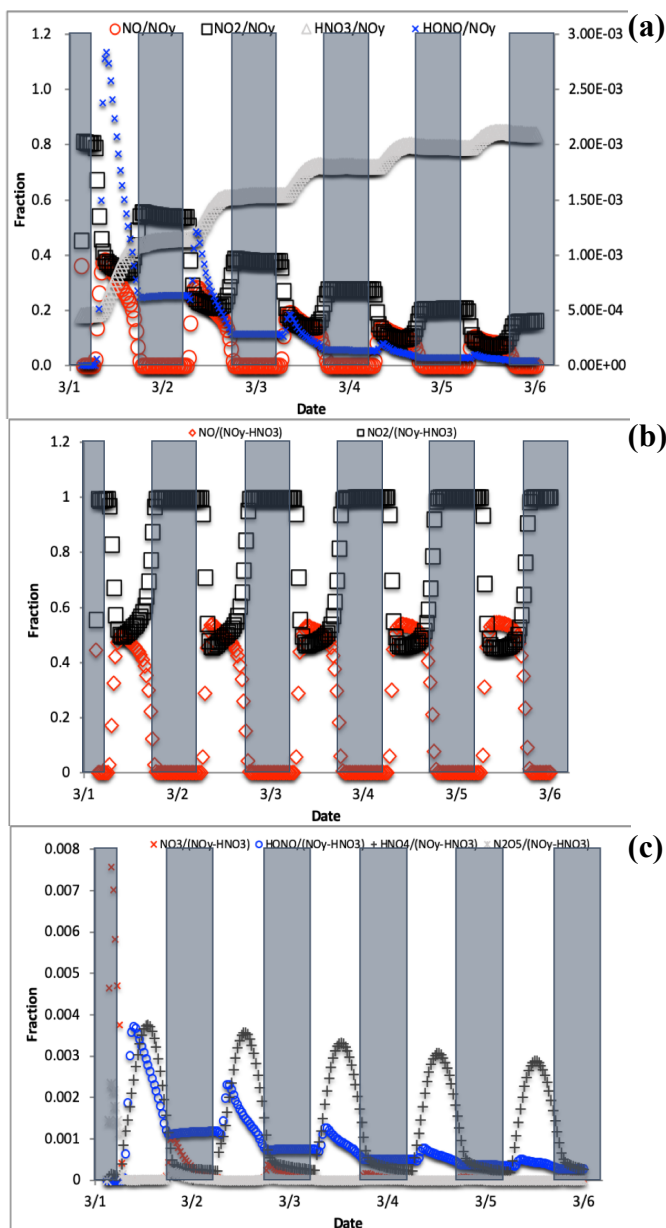


Figure 4. The change in  $f_{\text{NO}}$ ,  $f_{\text{NO}_2}$ ,  $f_{\text{NO}_3}$ , and  $f_{\text{HONO}}$  (right axis) over the 5-day simulation shows the transition from  $\text{NO}_y$  as mostly  $\text{NO}_x$  to predominately  $\text{HNO}_3$  (top, a). For reactive  $\text{NO}_y$  ( $\text{NO}_y - \text{HNO}_3$ ) large diurnal changes in  $f_{\text{NO}}$  and  $f_{\text{NO}_2}$  (middle, b) caused by photolysis minimize the other  $f_{\text{NO}_y}$  values, none of which exceeds 0.01 (bottom, c).

predicted  $\text{HNO}_3$   $\delta^{15}\text{N}$  value. Therefore, the only relevant KIE reactions that have  $\alpha \neq 1$  in  $i_{\text{N}}\text{RACM}$  mechanism are R39, R91-R97, R48 (Table S2b).

### 2.3.3 EIE relevant in $i_{\text{N}}\text{RACM}$ mechanism

While some EIE are naturally handled in the  $i_{\text{N}}\text{RACM}$  mechanism, such as the  $\text{NO}_2\text{--NO}_3\text{--N}_2\text{O}_5$  equilibrium, other potentially important N isotope exchange reactions are not directly expressed in RACM and must be considered. From a thermodynamic perspective, the EIE for any two N containing compounds can be calculated. The rate at which these compounds can achieve equilibrium, however, needs careful consideration. For example, the EIE for the isotope exchange reaction  $\text{NO} + {}^{15}\text{HNO}_3 \leftrightarrow {}^{15}\text{NO} + \text{HNO}_3$  has been calculated and measured [Brown and Begun, 1959]. Yet, steric considerations would suggest it would be very improbable for a gas phase reaction pathway or transition state to exist where two O atoms and a hydrogen from a  $\text{HNO}_3$  could quickly migrate to a NO molecule during a collision. The result is that isotope exchange for this gas phase reaction is likely kinetically too slow to be relevant but is valid in a highly concentrated liquid phase [Brown and Begun, 1959]. The larger the N containing molecule the more difficult it is to envision gas phase EIE occurring on a timescale comparable to the residence time tropospheric N of about a week. On the other hand, the isotope exchange reaction  $\text{NO} + {}^{15}\text{NO}_2 \leftrightarrow {}^{15}\text{NO} + \text{NO}_2$  rapidly occurs [Sharma et al., 1970] because it can form an ONONO ( $\text{N}_2\text{O}_3$ ) stable intermediate. As such,  $i_{\text{N}}\text{RACM}$  only considers N isotope equilibrium between NO,  $\text{NO}_2$ ,  $\text{NO}_3$ , and  $\text{N}_2\text{O}_5$ . Since the latter 3 compounds are already *chemically* equilibrated in RACM, they are by default isotopically equilibrated in  $i_{\text{N}}\text{RACM}$ . Therefore, the only new isotope exchange reaction added to  $i_{\text{N}}\text{RACM}$  was  $\text{NO} + {}^{15}\text{NO}_2 \leftrightarrow {}^{15}\text{NO} + \text{NO}_2$  (R238, R238a).

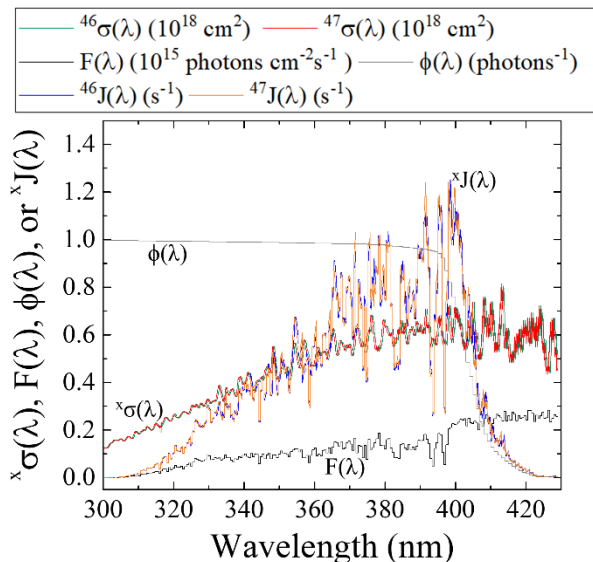


Figure 5. Literature reported  ${}^{46}\sigma(\lambda)$  [Vandaele et al., 2002]  $F(\lambda)$  (at SZA of  $60^\circ$ ; TUV model), and  $\text{NO}_2$   $\phi(\lambda)$  [Roehl et al., 1994] and calculated  ${}^{47}\sigma(\lambda)$  derived from the ZPE shift model for wavelengths relevant for tropospheric conditions for  $\text{NO}_2$  photolysis. From these parameters, both  ${}^{46}J(\lambda)$  and  ${}^{47}J(\lambda)$  have been calculated (Eq. 2).

## 2.4 Isotopologue fraction factors ( $\alpha$ ) used in $i_{\text{N}}\text{RACM}$

In this section we discuss the methodology used to determine the values for the relevant PHIFE, KIE, and EIE. These are reactions R1, R39, R48, R91-R97, and R238.

### 2.4.1 PHIFE derived $\alpha$ used in the $i_{\text{N}}\text{RACM}$ mechanism

The PHIFE for R1 was calculated using existing  $\text{NO}_2$  experimental photolysis cross-section of  ${}^{14}\text{NO}_2$  for tropospheric relevant wavelengths (300 to 450 nm) [Vandaele et al., 2002].

Using the experimentally determined  $\Delta ZPE$  for the  $^{15}\text{NO}_2$  isotopologue of  $29.79\text{ cm}^{-1}$  [Michalski et al., 2004], the  $^{47}\sigma(\lambda)$  was blue shifted by roughly 0.3 nm from the experimentally measured  $^{46}\sigma(\lambda)$  [Vandaele et al., 2002] (Fig. 5). The wavelength dependent actinic flux,  $F(\lambda)$ , was taken from the TUV model (NCAR) for solar zenith angles from 0 to 90° in 15° increments. The  $\phi(\lambda)$  values were taken from experimental data at 298 K [Roehl et al., 1994], and it was assumed that there is no significant quantum yield isotope effect. Based on these assumptions the  $^{46}J(\lambda)$  and  $^{47}J(\lambda)$  values were calculated (Fig. 5). An important feature of  $\text{NO}_2$  the wavelength dependent  $J$  include a peak near 390-400 nm that subsequently decreases at longer wavelengths until  $\text{NO}_2$  photolysis ceases beyond 420 nm due to a  $\phi = 0$  beyond this wavelength [Roehl et al., 1994]. Overall, the  $\text{NO}_2$  PHIFE  $\alpha$  value was found to be consistent for the wide range of solar zenith angles, ranging between 1.002 to 1.0042 with higher values occurring at lower solar zenith angles. We used an  $\alpha = 1.0042$  for daylight hours.

## 2.4.2 KIE derived $\alpha$ used in the $i_N\text{RACM}$ mechanism

### 2.4.2.1 KIE for the $\text{NO} + \text{O}_3$ reaction

The  $^{15}\alpha_{48}$  for the reaction  $\text{NO} + \text{O}_3 \rightarrow \text{NO}_2 + \text{O}_2$  reaction was determined by *ab initio* calculations [Walters and Michalski, 2016]. Generally, in a normal KIE the heavy  $^{15}\text{NO}$  would react with  $\text{O}_3$  slower than the light  $^{14}\text{NO}$ , which consistent with the calculated effect, however, it is relatively small ( $\epsilon = -6.7\text{‰}$  at 298 K). The  $^{15}\alpha_{48}$  was determined to have the following temperature dependent relationship [Walters and Michalski, 2016] over the temperature range of 220 to 320 K (Eq. (6)):

$$\alpha_{48} = (0.9822 * \exp(3.3523/T)) \quad \text{Eq. (6)}$$

### 2.4.2.2 KIE for the $\text{NO}_3 + \text{VOC}$ reactions

The most influential reactions that impacted the  $\delta^{15}\text{N}$  of  $\text{HNO}_3$  were the three reaction pathways that generate  $\text{HNO}_3$ . This is because the isotope effect associated with this last step is largely retained in the product  $\text{HNO}_3$  because photolysis of  $\text{HNO}_3$  back into photochemically active compounds that could re-scramble N isotopes is slow, effectively "locking in" these final isotope effects. Two gas phase reactions groups are important for  $\text{HNO}_3$  production. Nitric acid is produced mainly by R39 during the daytime [Seinfeld and Pandis, 1998] but this reaction is treated as an EIE as discussed below in the EIE section. During the nighttime, when the photolysis sink for  $\text{NO}_3$  vanishes,  $\text{NO}_3$  can react with VOCs to form  $\text{HNO}_3$  via hydrogen abstraction reactions [Atkinson, 2000]. Any individual  $\text{NO}_3 + \text{VOC}$  reaction had a small "relevance" for the  $\delta^{15}\text{N}$  values of  $\text{NO}_x$ , and  $\text{HNO}_3$ , but given there are 7 such reactions (R91-R97) their sum may be important.

The KIE for each of the  $\text{NO}_3 + \text{VOC} \rightarrow \text{HNO}_3$  reaction (R91-R97) was determined by assuming collisional frequency was the key KIE factor in such reactions. In these reactions (R91-R97)  $\text{NO}_3$  abstracts a hydrogen from a hydrocarbon, acting through a transition state involving the oxygen atoms in the nitrate radical C--H--ONO<sub>2</sub>. Since N is not directly participating in the bond formation it is classified as a secondary KIE [Wolfsberg, 1960]. Secondary KIE are typically much smaller than primary KIEs that occur at bond breaking/forming positions within a molecule [Wolfsberg, 1960]. Therefore, we assumed that the secondary KIE was negligible and did not factor into the  $\alpha$  values for these 7 reactions. On the other hand, isotope substitution does change the relative rate of collisions for N isotopologues because of the change in molecular mass. The

collisional frequency (Eq.7) for any of the NO<sub>3</sub> + VOC reaction pair was calculated assuming a hard sphere approximation via

$$A = \left[ \frac{8kT}{\pi\mu} \right]^{1/2} \pi d^2 \quad \text{Eq. (7)}$$

here  $\mu$  is the reduced mass of either NO<sub>3</sub> or <sup>15</sup>NO<sub>3</sub> and the specific hydrocarbon in a given reaction (R91-R97). When taking the isotopologue collision ratio, the constants, collision cross-section ( $d^2$ ), and temperature cancel out giving a temperature independent KIE of

$$\alpha = \frac{k_{15}}{k_{14}} = \frac{A_{15}}{A_{14}} = \sqrt{\frac{\mu_{15}}{\mu_{14}}} \quad \text{Eq. (8)}$$

The  $\alpha$  for each NO<sub>3</sub> + VOC reaction (R91-R97) as calculated using the hydrocarbon mass (Table S1b) and the NO<sub>3</sub> isotopologue masses (62, 63 amu) and using Eq. (8).

#### 2.4.3 EIE derived $\alpha$ used in the *i*<sub>N</sub>RACM mechanism

##### 2.4.3.1 EIE of NO + NO<sub>2</sub> exchange

The NO + NO<sub>2</sub> exchange was added to *i*<sub>N</sub>RACM by defining a forward and reverse reaction (R238, R238a) and an equilibrium constant  $K_{238} = k_{238}/k_{238a} = \alpha$ . The forward rate constant ( $k_{238}$ ) was based on the NO-NO<sub>2</sub> isotope exchange rate determined by Sharma et al. ( $3.6 \cdot 10^{14} \text{ cm}^3 \text{ s}^{-1} \text{ molecule}^{-1}$ ). The reverse rate was calculated using  $k_{238a} = k_{238}/\alpha$ . The temperature-dependent for EIE of NO + NO<sub>2</sub> exchange (Eq. 9) was calculated using quantum mechanical techniques [Walters and Michalski, 2015] that matched well with recent experimental values [Walters et al., 2016].

$$\alpha_{238} = 0.9771 \cdot \exp(18.467/T) \quad \text{Eq. (9)}$$

##### 2.4.3.2 EIE used in the NO<sub>2</sub> + OH reaction

The <sup>15</sup> $\alpha_{39}$  for the NO<sub>2</sub>+OH+M → HNO<sub>3</sub> reaction (R39) was determined by assuming equilibrium between NO<sub>2</sub> and HNO<sub>3</sub>. The third body and the negative temperature dependence of the rate constant shows that, similar to O<sub>3</sub> formation, this reaction is an association reaction [Golden and Smith, 2000]. It proceeds through an excited intermediate, \*HNO<sub>3</sub>, that can undergo collisional deactivation by a third body M (Eq.10).

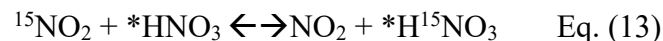


in which  $k_f$  and  $k_r$  are the forward and reverse rate constants for the association step and  $k_q$  is the rate constant for collisional quenching and deactivation of the activated complex. We have calculated that  $k_r/k_q$  is on the order of 5.5 (see SA) thus the assumption about reactant-complex isotopic equilibrium appears to be valid since only a single decomposition would isotopic equilibrium. The HNO<sub>3</sub> production rate constant is then  $k_f k_d [M] / k_r = K_{eq} k_d [M]$ . This general form can be used to write two isotopologue equilibrium constants  $K$

$$K_{39} = [*HNO_3]/([NO_2][OH]) = k_{39f}/k_{39r} \quad \text{Eq. (11)}$$

$$K_{39a} = [*H^{15}NO_3]/([^{15}NO_2][OH]) = k_{39af}/k_{39ar} \quad \text{Eq. (12)}$$

Since •OH is not participating in the N isotope chemistry, these two EIE effectively reduces the isotope chemistry to the temperature dependent <sup>15</sup>N EIE



$$K_{39a}/K_{39} = \alpha_{HNO_3/NO_2} = \beta_{HNO_3}/\beta_{NO_2} \quad \text{Eq. (14)}$$

The fundamental vibration frequencies for HNO<sub>3</sub>\* were taken to be the same as ground state HNO<sub>3</sub>, similar to RRKM theory approaches used to calculate the uni-molecular decay rate of HNO<sub>3</sub>\* [Golden and Smith, 2000]. The temperature-dependent β<sub>HNO<sub>3</sub></sub> and β<sub>NO<sub>2</sub></sub> values for this exchange were taken from [Walters and Michalski, 2015]. Since the reaction has a negative activation energy and has a fairly rapid rate constant at 101 kPa, (1 x 10<sup>11</sup> cm<sup>-3</sup> s<sup>-1</sup>) and the isotope effect due to the collisional deactivation frequency (Eq. 7) is minimal (~2‰) compared to the equilibrium effect (~40‰), the deactivation rate constants k<sub>d</sub> were set equal (k<sub>d14</sub>/k<sub>d15</sub>=1). Setting k<sub>r14</sub>= k<sub>r15</sub>, and using the α<sub>HNO<sub>3</sub>/NO<sub>2</sub></sub> equilibrium value the k<sub>39a</sub> for the <sup>15</sup>NO<sub>2</sub> + OH → H<sup>15</sup>NO<sub>3</sub> reaction is

$$K_{39a} = \alpha_{HNO_3/NO_2} (K_{39}) \quad \text{Eq. (15)}$$

The temperature dependence of α<sub>HNO<sub>3</sub>/NO<sub>2</sub></sub> is derived from the tables in [Walters and Michalski, 2015] and α<sub>39</sub> is then:

$$\alpha_{39} = (0.973 * \exp(19.743/T)) \quad \text{Eq. (16)}$$

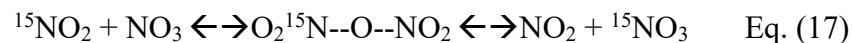
For typical tropospheric temperatures the α<sub>HNO<sub>3</sub>/NO<sub>2</sub></sub> 1.040 suggesting the δ<sup>15</sup>N of HNO<sub>3</sub> produced by the NO<sub>2</sub> + OH reaction will be +40‰ relative to tropospheric NO<sub>2</sub>. This α value is larger and opposite the sign of the <sup>15</sup>α = 0.9971 assumed by Freyer et al. (1991). Freyer's α was approximated by the using reduced mass of the OH-NO<sub>2</sub> activated complex. There two problems with this approach. First, the activation complex's reduced mass approximation should be viewed in terms as the *decomposition* rate constant, not the product formation rate constant as assumed by Freyer, because transition state theory assumes equilibrium between the stable *reactants* and the transition state [Bigeleisen and Wolfsberg, 1958; Wolfsberg et al., 2010]. In other words, Freyer's α = 0.9971 should indicate that the <sup>15</sup>NO<sub>2</sub>-OH decomposes more slowly than <sup>14</sup>NO<sub>2</sub>-OH and therefore more likely to form HNO<sub>3</sub> at +2.9‰ (not -2.9‰ determined in Freyer). Secondly, the reduced mass approximation of the complex pair ignores the thermodynamic contribution of the reactants and the vibrations in the transitions state other than the bond forming (imaginary) vibration. Our approach overcomes both of these assumptions and incorporates the temperature dependence of the EIE for this reaction.

#### 2.4.3.3 EIE used in heterogeneous reactions of N<sub>2</sub>O<sub>5</sub>

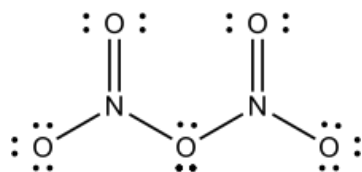
During the nighttime, the heterogeneous HNO<sub>3</sub> formation pathway becomes important [Chang et al., 2011; Dentener and Crutzen, 1993; Riemer et al., 2003]. During the night, NO is nearly completely oxidized to NO<sub>2</sub> leading to the build-up of the NO<sub>3</sub> radical (R48), the formation of N<sub>2</sub>O<sub>5</sub> (R53), and heterogeneous N<sub>2</sub>O<sub>5</sub> hydrolysis becomes a major source of HNO<sub>3</sub> production

(discussed below). This is particularly true in regions that have high NO<sub>x</sub> mixing ratios and large aerosol surface areas such as urban centers [Chang *et al.*, 2011; Riemer *et al.*, 2003]. In order to assess the <sup>15</sup>N partitioning of this reaction pathway, both EIE and KIE were considered.

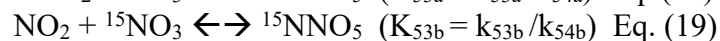
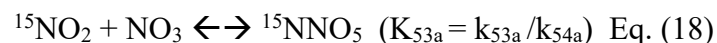
It was assumed that the fractionation factor for the N<sub>2</sub>O<sub>5</sub> → 2HNO<sub>3</sub> reaction was mainly controlled by nighttime equilibrium between N<sub>2</sub>O<sub>5</sub> and NO<sub>2</sub>/NO<sub>3</sub> (R53, R54). When factoring the isotopologue dynamics, this equilibrium can be viewed as an EIE via



here <sup>15</sup>N<sub>2</sub>O<sub>5</sub> is represented as the transition state O<sub>2</sub><sup>15</sup>N--O--NO<sub>2</sub> to highlight the relative ease of N isotope exchange via oxygen migration during N<sub>2</sub>O<sub>5</sub> formation and decomposition. The symmetry of <sup>15</sup>NNO<sub>5</sub> and N<sup>15</sup>NO<sub>5</sub> is also why they were not treated as isotopomers since they are structurally identical.



The N<sub>2</sub>O<sub>5</sub> equilibrium in the RACM model is dealt with as a forward reaction R53 (*k*<sub>53</sub>) and a decomposition reaction R54 (*k*<sub>54</sub>) that are derived from the measured equilibrium constant (*K*<sub>53</sub>) = (*k*<sub>53</sub>/*k*<sub>54</sub>). In *i*<sub>N</sub>RACM the N<sub>2</sub>O<sub>5</sub> isotopologue has 2 formation pathways, with two forward rate constants (*k*<sub>53 a,b</sub>) and two decomposition rate constants (*k*<sub>54 a,b</sub>) that were used to write their respective equilibrium constants *K*



Dividing *K*<sub>53a</sub> and *K*<sub>53b</sub> by *K*<sub>53</sub> yields isotopologue product and reactant ratios that can be evaluated using β(*α*) values from Walters and Michalski (2015). These were used to determine the *α* value for the N<sub>2</sub>O<sub>5</sub> isotopologue equilibrium, which are simply a function of the formation and decomposition rate constants and temperature

$$\begin{aligned} K_{53a}/K_{53} &= (^{15}\text{NNO}_5/\text{N}_2\text{O}_5)(\text{NO}_2/^{15}\text{NO}_2)(\text{NO}_3/\text{NO}_3) = \beta_{\text{N}_2\text{O}_5}/\beta_{\text{NO}_2} \\ &= \alpha_{\text{N}_2\text{O}_5/\text{NO}_2} = k_{53a}/k_{53} \times k_{54}/k_{54a} \quad \text{Eq. (20)} \end{aligned}$$

$$\begin{aligned} K_{53b}/K_{53} &= (^{15}\text{NNO}_5/\text{N}_2\text{O}_5)(\text{NO}_3/^{15}\text{NO}_3)(\text{NO}_2/\text{NO}_2) = \beta_{\text{N}_2\text{O}_5}/\beta_{\text{NO}_3} \\ &= \alpha_{\text{N}_2\text{O}_5/\text{NO}_3} = k_{53b}/k_{53} \times k_{54}/k_{54b} \quad \text{Eq. (21)} \end{aligned}$$

The N<sub>2</sub>O<sub>5</sub> decomposition rate constants were arbitrarily set to be equal (*k*<sub>54</sub> = *k*<sub>54a</sub> = *k*<sub>54b</sub>) and the decomposition rate constants were then derived using the temperature dependent *α* values

$$k_{53a} = k_{53}(\alpha_{\text{N}_2\text{O}_5/\text{NO}_2}) \quad \alpha_{\text{N}_2\text{O}_5/\text{NO}_2} = 1.0266 \quad (298 \text{ K}) \quad \text{Eq. (22)}$$

$$k_{53b} = k_{53}(\alpha_{\text{N}_2\text{O}_5/\text{NO}_3}) \quad \alpha_{\text{N}_2\text{O}_5/\text{NO}_3} = 1.0309 \quad (298 \text{ K}) \quad \text{Eq. (23)}$$

The  $\alpha$  for doubly substituted  $^{15}\text{N}_2\text{O}_5$  isotopologue was determined using  $\alpha = \beta_{^{15}\text{N}_2\text{O}_5}/\beta_{\text{NO}_2}\beta_{\text{NO}_3}$  and the value for  $\beta_{^{15}\text{N}_2\text{O}_5}$  (1.272) was approximated using the principle of the geometric mean [Bigeleisen, 1958; Snyder *et al.*, 1999], yielding a temperature independent  $\alpha = 1.057$ . However, the  $\text{N}_2\text{O}_5$  system is insensitive to this  $\alpha$  value because the low probability of a  $^{15}\text{N} + ^{15}\text{N}$  reaction ( $1.5 \times 10^{-5}$ ) relative to a  $^{14}\text{N} + ^{15}\text{N}$  reaction ( $4 \times 10^{-3}$ ), thus the small temperature dependence was also ignored.

Because RACM is a gas phase chemical mechanism, it does not include heterogeneous reactions of  $\text{N}_2\text{O}_5$  on aerosols, which would limit  $i_{\text{N}}\text{RACM}$  to accurately predict the  $\delta^{15}\text{N}$  values, particularly at night. Gas chemical mechanisms are often used in larger 1, 2, and 3-D chemical transport models that usually also include aerosol modules that calculate heterogeneous chemistry using inputs from the gas phase chemical mechanism (i.e.  $\text{N}_2\text{O}_5$  concentrations). However, if the objective is to use a 0-D chemical box model to simulate local chemistry the  $\text{N}_2\text{O}_5$  heterogeneous hydrolysis will need to be included.  $i_{\text{N}}\text{RACM}$  was modified to use a first order rate constant to calculate  $\text{N}_2\text{O}_5$  heterogeneous hydrolysis [Yvon *et al.* 1996; Riemer *et al.*, 2003]. The rate constant is a function of  $\text{N}_2\text{O}_5$  molecular speed ( $c$ ), the  $\text{N}_2\text{O}_5$  uptake coefficient ( $\gamma$ ) and the aerosol surface area density  $S$ .

$$-d\text{N}_2\text{O}_5/dt = d0.5\text{HNO}_3/dt = k_{\text{N}_2\text{O}_5}[\text{N}_2\text{O}_5] = R239 \quad k_{\text{N}_2\text{O}_5} = \frac{1}{2}c \gamma S \quad \text{Eq. (24)}$$

The  $k_{\text{N}_2\text{O}_5}$  values were assessed based on the different pollutant loadings and emission scenarios (Fig. 6). The  $k_{\text{N}_2\text{O}_5}$  was calculated as a function of  $\gamma$  [Anttila *et al.*, 2006; Bertram & Thornton, 2009; Davis *et al.*, 2008; Riemer *et al.*, 2003; Riemer *et al.*, 2009] and  $S$  [Cai *et al.*, 2018; Kuang *et al.*, 2010; McMurry *et al.*, 2005; Petäjä *et al.*, 2009; Qi *et al.*, 2015] values that span clean to highly polluted environments. This range yielded  $k_{\text{N}_2\text{O}_5} = 1, 0.1, \text{ and } 0.01$  for high, medium, and low polluted environments (Fig. 6).

Only the uptake coefficient ( $\gamma$ ) and molecular speed ( $c$ ) could have a KIE during aerosol uptake of  $\text{N}_2\text{O}_5$  (R239, R239a, R239b). The  $\gamma$  term was ignored because *ab initio* work suggests that  $\text{N}_2\text{O}_5$  hydrolysis activates through hydrogen bonding between water molecules on the aerosol surface and O atom in the  $\text{N}_2\text{O}_5$  [Snyder *et al.*, 1999] making it a secondary (small) KIE for N. The  $c$  term is a function of the root of the  $\text{N}_2\text{O}_5$  molecular mass and when the ratio is taken there is no temperature dependence yielding  $\alpha_{239a} = (108/109)^{0.5} = 0.995$  and  $\alpha_{239b} = (108/110)^{0.5} = 0.9909$ .

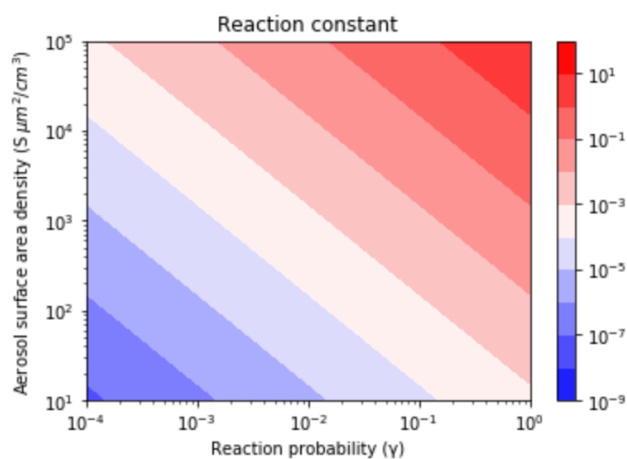


Figure 6. Contour lines of the same  $k_{\text{N}_2\text{O}_5}$  values as a function of  $\gamma$  and  $S$  values. The  $\gamma$  values depend on aerosol composition and range from  $3.8 \times 10^{-5}$  (relatively dry sulfuric acid) to 1 (aqueous aerosol in the winter polar stratosphere).  $S$  values are a function of aerosol number density and size distribution and range from 52 (low scavenging rate, low particle growth rate) to 1140.1 (high scavenging rate, high particle growth rate).



An online version of this  $i_N$ RACM model is available for public use at <https://mygeoHub.org/tools/sbox/>

#### 2.4.4 Addition of O<sub>3</sub> deposition to $i_N$ RACM

Photochemical mechanisms such as RACM are validated by comparing model predictions with observed trace gas concentration evolution in chambers studies, which has its limitations. For example, Stockwell et. al. compared RACM, RADM2, and SPARC mechanisms ability to predict trace gases concentrations (e.g. O<sub>3</sub>, NO<sub>2</sub>, toluene) with those observed in chamber experiments [see Stockwell et. al., Fig 3-9] and achieve good agreement between the model and experiments. These experiment-model comparisons essentially validate the rate constant assumptions in the chemical mechanism. Box models are, however, limited in their ability to predict real world concentrations because many do not account for pollutant deposition (dry or wet) since these are handled when the mechanism is incorporated into 1, 2, and 3D transport models. Similarly, dilution by of trace gases due to vertical (or horizontal) transport is typically not incorporated into 0-box models. This can lead to the buildup (or depletion) of key oxidants, particularly O<sub>3</sub> [see Fig. 6 in Stockwell et.al.]. This in turn will significantly alter NO<sub>x</sub> oxidation pathways, and since the  $\delta^{15}\text{N}$  in  $i_N$ RACM is effectively a function on changing oxidation pathways, this would impact  $i_N$ RACM ability to accurately predict the observations of  $\delta^{15}\text{N}$  in the real world. In order to eliminate this bias, we added a O<sub>3</sub> deposition reaction and adjusted the rate until O<sub>3</sub> mixing ratios were inline with typical suburban mixing ratios (20-30 ppb) and exhibited a typical O<sub>3</sub> diurnal mixing ratio variation, low nighttime/high midday, that are observed in most environments (Fig S2). This results in simulated daytime maximum OH concentrations on the order of  $\sim 8 \times 10^6$  molecules cm<sup>-3</sup> and daytime average of  $\sim 2 \times 10^6$  molecules cm<sup>-3</sup> (Fig S2) that are typical of overserved concentrations in urban and suburban environments [see refs. in the review by Monks, 2005]. This gives us confidence that  $i_N$ RACM is accurately capturing boundary layer photochemistry and can be used to predict  $\delta^{15}\text{N}$  in NO<sub>y</sub> compounds.

#### 2.4.5 $i_N$ RACM simulations

A number of  $i_N$ RACM simulations were run with two different purposes. The first set of simulations iteratively changed the  $\alpha$  values from 1 to their values discussed above. These simulations aimed at investigating the importance of each  $\alpha$  as they aggregated together. These include photolysis only, Leighton cycle, daytime chemistry, night-time chemistry, and full chemistry using the same test case (Table S3a-f). These were run with all  $\alpha$ 's activated but with varied initialized chemistry and primary pollutant emissions.

### 3.0 Results and Discussion

It is important to first test  $i_N$ RACM by turning on and off individual relevant isotope effects and then combining their cumulative effects. This is advantageous relative to simply running the full mechanism under different pollution scenarios because it would be a challenge to disentangle which isotope effects in the full mechanism were mainly responsible for  $\delta^{15}\text{N}$  change in NO<sub>x</sub>, HONO, or HNO<sub>3</sub> without such a systematic investigation. For example, it is likely that the  $\delta^{15}\text{N}$  value of NO<sub>2</sub> will be a significant factor in the  $\delta^{15}\text{N}$  value of HNO<sub>3</sub> because it is the reactant in R39 and R239. Thus, understanding which isotope effects control the  $\delta^{15}\text{N}$  of NO<sub>2</sub> helps with interpreting the  $\delta^{15}\text{N}$  value of HNO<sub>3</sub> and vice versa. Thus, this discussion section is divided into 3

sections. The first is the examination of the relevant isotope effects occurring during daytime photochemistry and their impact on  $\text{NO}_x$ , HONO, and  $\text{HNO}_3$   $\delta^{15}\text{N}$  values. Secondly, is the examination of the relevant isotope effects occurring during nighttime chemistry (EIE and KIE) and their effect on  $\text{NO}_x$ , HONO, and  $\text{HNO}_3$   $\delta^{15}\text{N}$  values. These first two discussion sections focus mainly on the relative importance of each isotope effect when the photochemical conditions are constant. Finally, the full  $i_{\text{N}}\text{RACM}$  mechanism will be tested under different atmospheric conditions such as variations in trace gas concentrations, aerosol loading, and hours of sunlight. This tests how changes in photochemical oxidation pathways results in difference in the  $\delta^{15}\text{N}$  values of  $\text{NO}_x$ , HONO, and  $\text{HNO}_3$ .

### 3.1 The $\delta^{15}\text{N}$ of $\text{NO}_x$ , HONO, and $\text{HNO}_3$ due to daytime chemistry

The role that daytime chemistry plays in determining the  $\delta^{15}\text{N}$  values of  $\text{NO}_x$ , HONO, and  $\text{HNO}_3$  was investigated by iteratively adding relevant fractionation factors to  $i_{\text{N}}\text{RACM}$ . The sensitivity of  $\text{NO}_x$ , HONO, and  $\text{HNO}_3$   $\delta^{15}\text{N}$  values to  $\text{NO}_2$  photolysis (R1a) was tested. The initial trace gas concentrations and emissions were set to the March 1 test cases (Table S3 a-f) and simulations were run with, and without,  $\text{NO}$  emissions. All subsequent test simulations will also use the March 1 test case in order to have a consistent comparison of  $\delta^{15}\text{N}$  values between different simulations. It is noted that the initial  $\text{HNO}_3$  and  $\text{O}_3$  mixing ratios are set to zero and that the start time of the simulations is 3 a.m. The main daytime only effects will be  $\text{NO}_2$  photolysis (R1),  $\text{O}_3$  oxidation (R8) and reaction OH (R39) since both photolysis and OH chemistry is only relevant during the daytime. However,  $\text{NO}_x$  isotope exchange and  $\text{NO} + \text{O}_3$  will also play a vital role despite no being exclusively daytime reactions.

#### 3.1.1 The $\delta^{15}\text{N}$ values of $\text{NO}_x$ , HONO, and $\text{HNO}_3$ due to the photolysis only

The simulations with only R1 isotope effect activated (with  $\text{NO}_x$  emissions) shows a clear diurnal cycle in  $\text{NO}_x$  and HONO  $\delta^{15}\text{N}$  values and a multiday trend moving towards an approximate steady state for  $\text{HNO}_3$   $\delta^{15}\text{N}$  values, which can be explained by the PHIFE (Fig. 7a). Initially all  $\text{NO}_y$  has  $\delta^{15}\text{N}$

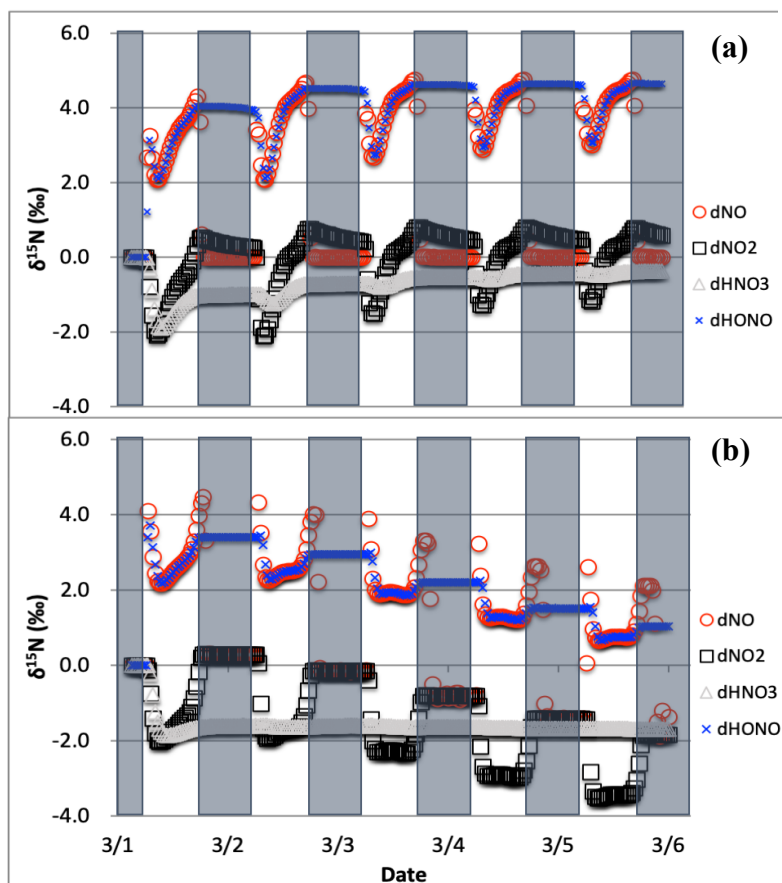


Figure 7. The  $\delta^{15}\text{N}$  values of  $\text{NO}$  (O),  $\text{NO}_2$  ( $\square$ ) HONO (x), and  $\text{HNO}_3$  ( $\square$ ) with only the photolysis isotope fractionations active. The 5-day simulation was under the conditions list in Table S3a-b. The gray boxes span night hours and the white span daytime. The top (a) is the simulation with  $\text{NO}_x$  emissions and the bottom (b) is without  $\text{NO}_x$  emissions.

of zero (by default) and there is no photolysis at 3 am. At sunrise the  $\delta^{15}\text{N}$  value of  $\text{NO}_2$  goes negative and  $\text{NO}$  value positive since  $^{15}\text{NO}_2$  is preferentially photolyzed ( $\alpha_{\text{R1}} = 1.0042$ ). The difference between the  $\delta^{15}\text{N}$  values of  $\text{NO}$  and  $\text{NO}_2$  ( $\Delta\delta^{15}\text{N}_{\text{NO-NO}_2} = \delta^{15}\text{N}_{\text{NO}} - \delta^{15}\text{N}_{\text{NO}_2}$ ) at all times during the day is 4‰, which is the  $\epsilon_{\text{R1a}}$  value. During the night both the  $\text{NO}$  and  $\text{NO}_2$   $\delta^{15}\text{N}$  values approach 0‰ because most  $\text{NO}$  is oxidized to  $\text{NO}_2$  and  $\text{NO}$  emissions (0‰) dominate the  $\text{NO}$  nighttime budget (relative to residual day  $\text{NO}$ ). Over the weeklong simulation, the  $\text{NO}_x$   $\delta^{15}\text{N}$  value slowly increases by about one per mil. This is because  $^{15}\text{N}$  depleted  $\text{NO}_2$  is converted into  $\text{HNO}_3$  leaving the residual  $\text{NO}_x$   $^{15}\text{N}$  enriched. This is also the reason for the  $\delta^{15}\text{N}$  values of  $\text{HNO}_3$  that initially mimic the daytime  $\text{NO}_2$  values and trends towards 0‰ by the end of the simulation week. The  $\delta^{15}\text{N}$  values of  $\text{HONO}$  mimics the  $\text{NO}$  values during the daytime since the main reaction pathway forming  $\text{HONO}$  is  $\text{OH} + \text{NO}$ , which peaks in the morning (~10:00).  $\text{HONO}$  retains the evening  $\delta^{15}\text{N}$  values through the night since most of the  $\text{HONO}$  is destroyed in the afternoon via photolysis and again follows  $\text{NO}$   $\delta^{15}\text{N}$  the next morning as its production again reaches a maximum (Fig. 7a).

The simulation without  $\text{NO}$  emissions shows a similar behavior but with some clear differences relative to the emission case. The  $\text{NO}_x$  and  $\text{HONO}$   $\delta^{15}\text{N}$  values exhibit the same diurnal  $\Delta\delta^{15}\text{N}_{\text{NO-NO}_2} = 4$ ‰ value. Unlike the emission case, however, the diurnal  $\text{NO}_x$   $\delta^{15}\text{N}$  value peaks and troughs trend downward during the week-long simulation, with  $\text{NO}$  approaching 0‰ and  $\text{NO}_2$  approaching -4‰. The  $\text{HNO}_3$   $\delta^{15}\text{N}$  values reach roughly a steady state value of -1.7‰ after about a day and  $\text{NO}_x$  is ~ -1.8‰ (Fig. 7b). This difference between the emission and non-emission case is a consequence of isotope mass balance ( $f_x =$  mole fraction of compound  $x$  relative to total  $\text{NO}_y$ ).

$$\delta^{15}\text{N}_{\text{total}} = 0 = f_{\text{NO}_x} \cdot \delta^{15}\text{N}_{\text{NO}_x} + f_{\text{HNO}_3} \cdot \delta^{15}\text{N}_{\text{NHNO}_3} + f_{\text{ONIT}} \cdot \delta^{15}\text{N}_{\text{ONIT}} \quad \text{Eq. (25)}$$

The positive  $\delta^{15}\text{N}$   $\text{NO}_y$  compound that effectively offsets the -1.7‰ in  $\text{HNO}_3$  and -1.8‰ in  $\text{NO}_x$  is organic nitrate that is +2‰ and makes about half the  $\text{NO}_y$  pool and is roughly equal to  $\text{HNO}_3 + \text{NO}_x$  ( $f_{\text{NO}_x} = 0.11$ ,  $f_{\text{HNO}_3} = 0.36$ ,  $f_{\text{ONIT}} = 0.53$ ). In the  $\text{NO}_x$  emission case only about 5% of  $\text{NO}_y$  is as organic nitrate ( $f_{\text{NO}_x} = 0.17$ ,  $f_{\text{HNO}_3} = 0.78$ ,  $f_{\text{ONIT}} = 0.05$ ) indicating a shift in oxidation pathways when  $\text{NO}$  and  $\text{VOCs}$  are emitted during the simulation relative to when they are not. In the emissions case the  $\text{NO}_x$  mixing ratios at the end of the simulation are actually slightly higher than their initial ratios, in contrast to the no  $\text{NO}_x$  emission case where 90% of  $\text{NO}_x$  has been lost via oxidation into organic nitrate and  $\text{HNO}_3$ . This loss of  $\text{N}$  in the no emission scenario effectively shuts down the oxidation chemistry. For example, the day 5 mixing ratio of  $\text{O}_3$  is 45 ppb<sub>v</sub> (reasonable) for the emission case but only 2 ppb<sub>v</sub> for the non-emission case (unreasonable). Therefore, we exclude no-emission simulations for the chemistry analysis discussed in this section and restrict them to the no emission simulations

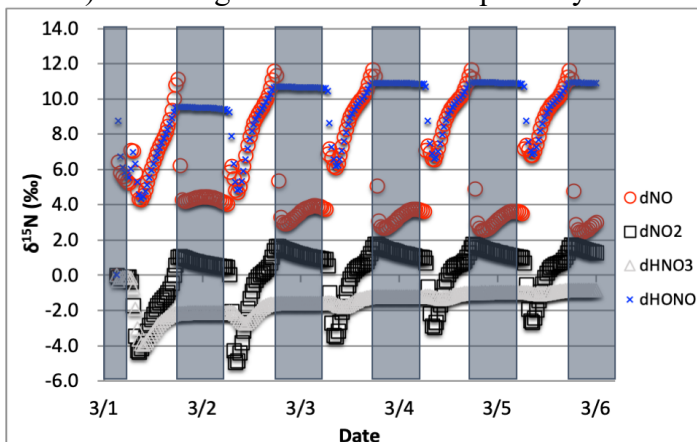


Figure 8. The  $\delta^{15}\text{N}$  values of  $\text{NO}_x$ ,  $\text{HONO}$ , and  $\text{HNO}_3$  when isotope effects associated R1 and R48 are combined, with  $\text{NO}_x$  emission. The 5-day simulation was under the conditions list in Table S3a-b. The diurnal patterns are reflecting the relative importance of photolysis and  $\text{O}_3$  chemistry during the day and night.

to 48 hours in the final test case analysis (See section 4).

### 3.1.2 The $\delta^{15}\text{N}$ values of $\text{NO}_x$ , HONO, and $\text{HNO}_3$ due to the combined Leighton cycle

The simulations with both  $\text{NO}_2$  photolysis (R1) and  $\text{O}_3 + \text{NO}$  (R48) isotope effects active shows similar diurnal and multiday trends as the photolysis only simulations, they are just slightly amplified (Fig. 8). The daytime  $\Delta\delta^{15}\text{N}_{\text{NO-NO}_2}$  is now  $\sim 9.5\text{‰}$ , which is close to the additive of the two isotope effects ( $\epsilon_{48a} = -6.7\text{‰}$ ,  $\epsilon_{R1a} = 4.2\text{‰}$ ). This is logical since  $^{15}\text{NO}$  is reacting with  $\text{O}_3$  slower than  $^{14}\text{NO}$ , preferentially leaving behind  $^{15}\text{NO}$  and thus the higher NO  $\delta^{15}\text{N}$  value. The  $\text{HNO}_3$   $\delta^{15}\text{N}$  values reach the mean of the daytime  $\text{NO}_2$   $\delta^{15}\text{N}$  values via the  $\text{NO}_2 + \text{OH}$  reaction. The slight ( $1\text{‰}$ ) upward trend of  $\text{NO}_x$  and  $\text{HNO}_3$  are due to isotope mass balance as detailed in the photolysis only case. Similar to the photolysis only case the  $\delta^{15}\text{N}$  of HONO is mimicking daytime NO  $\delta^{15}\text{N}$  values.

### 3.1.3 The $\delta^{15}\text{N}$ values of $\text{NO}_x$ , HONO, and $\text{HNO}_3$ due to the combined Leighton cycle and $\text{NO}_x$ isotope exchange

The  $\delta^{15}\text{N}$  values of  $\text{NO}_x$  produced when both the Leighton cycle and  $\text{NO}_x$  isotope exchange are active exhibit a very dynamic diurnal range that is a function of the  $\text{NO}_x$  mixing ratios. At high  $\text{NO}_x$  mixing ratios (150 ppb, 1/3 NO, 2/3  $\text{NO}_2$ , Fig. 9a) the  $\Delta\delta^{15}\text{N}_{\text{NO-NO}_2}$  is  $-40\text{‰}$  at night as expected for  $\text{NO}_x$  isotopic equilibrium ( $\epsilon_{\text{NO/NO}_2} = -40\text{‰}$  at 298K). During the daytime the  $\Delta\delta^{15}\text{N}_{\text{NO}_x}$  shifts  $-30$  to  $-35\text{‰}$  as the photolysis and  $\text{O}_3$  isotope effects begin to influence the  $\Delta\delta^{15}\text{N}_{\text{NO-NO}_2}$ .  $\text{HNO}_3$   $\delta^{15}\text{N}$  values during the high  $\text{NO}_x$  mixing ratio simulation initially follow the  $\delta^{15}\text{N}$  of  $\text{NO}_2$  (via  $\text{NO}_2 + \text{OH}$ ) before approaching  $0\text{‰}$ , the defined  $\text{NO}_x$  source values.

At low  $\text{NO}_x$  mixing ratios (1.5 ppb, 1/3 NO, 2/3  $\text{NO}_2$ , Fig. 9c) the  $\Delta\delta^{15}\text{N}_{\text{NO-NO}_2}$  and  $\text{HNO}_3$   $\delta^{15}\text{N}$  is very different from the high  $\text{NO}_x$  simulation. The nighttime  $\Delta\delta^{15}\text{N}_{\text{NO-NO}_2}$  ranges from  $-15$  to  $-20\text{‰}$  and during the daytime it is around  $+7\text{‰}$ , while the  $\text{HNO}_3$   $\delta^{15}\text{N}$  values hover around zero throughout the simulation. The difference between the  $\text{NO}_y$   $\delta^{15}\text{N}$  values in the high and low  $\text{NO}_x$  cases can be explained as a competition between the  $\text{NO}_x$  EIE and the Leighton isotope effect. At high  $\text{NO}_x$  mixing ratios, the  $\text{NO}_x$  EIE achieves equilibrium quickly at night ( $\Delta\delta^{15}\text{N}_{\text{NO-NO}_2} = -40$ )

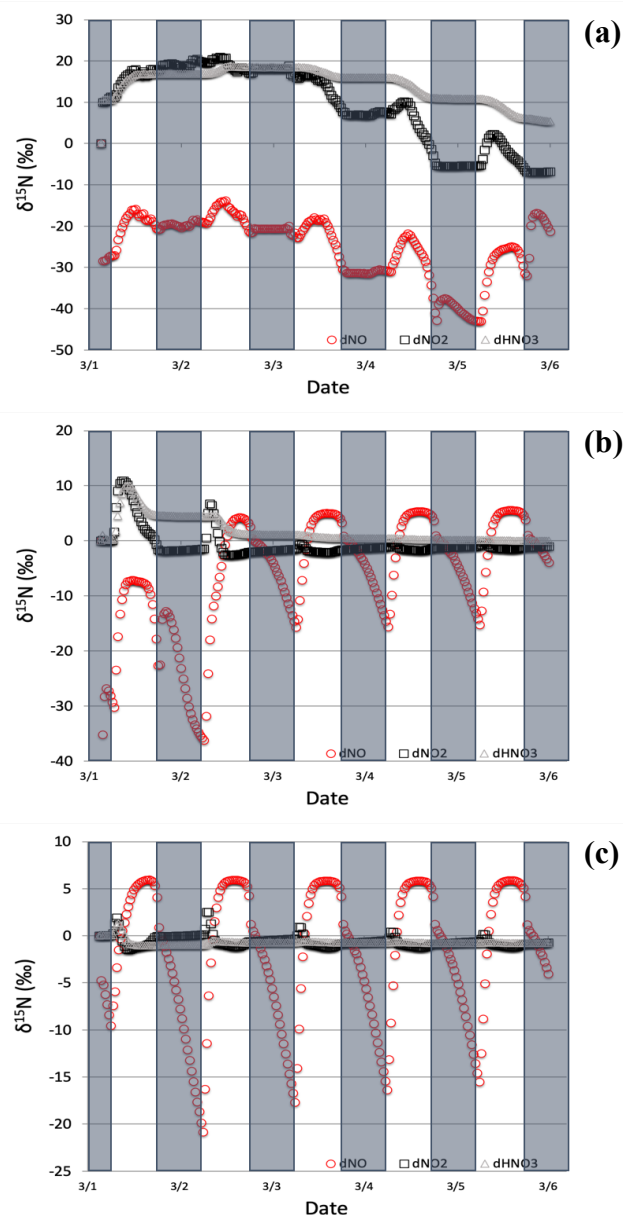


Figure 9. The  $\delta^{15}\text{N}$  values of  $\text{NO}_x$  and  $\text{HNO}_3$  when isotope effects in R1, R48, and R238 are included under high (top, a), medium (middle, b), and low (bottom, c)  $\text{NO}_x$  scenarios. The 5-day simulation was under the conditions list in Table S3d-f. The  $\text{NO}_y$   $\delta^{15}\text{N}$  values are mainly controlled by  $\text{NO}_x$  isotope exchange (R238) under high  $\text{NO}_x$  conditions and Leighton (R1 + R58) under low  $\text{NO}_x$  conditions.

because the rate of  $\text{NO}_x$  isotope exchange (R238) is proportional to its concentration. In contrast, isotope exchange is slow in the low  $\text{NO}_x$  case and the time scale to reach equilibrium is much longer. Indeed, at the low  $\text{NO}_x$  mixing ratios the nighttime equilibrium only reaches about 40-50% of completion by 6:30. Afterwards sunlight begins to erase the  $\text{NO}_x$  EIE effect until around noon when the  $\delta^{15}\text{N}$  values of  $\text{NO}$  is mostly due to the Leighton effect and only a small contribution from EIE (about 5%). For intermediate  $\text{NO}_x$  mixing ratio case (15 ppb, 1/3  $\text{NO}$ , 2/3  $\text{NO}_2$ , Fig. 9b) the diurnal and week-long  $\text{NO}_y$   $\delta^{15}\text{N}$  trends fall somewhere in between the high and low  $\text{NO}_x$  simulations.

The changes in  $\delta^{15}\text{N}$  values of  $\text{HNO}_3$  during the March 1 simulations at differing  $\text{NO}_x$  mixing ratios can be explained in terms of  $\text{HNO}_3$  production pathways. Over the course of day 1 the  $\delta^{15}\text{N}$  of  $\text{HNO}_3$  mirrors that of  $\text{NO}_2$  because  $\text{HNO}_3$  produced by  $\text{NO}_2 + \text{OH}$  (R39), thus the product  $\text{HNO}_3$   $\delta^{15}\text{N}$  values are similar to those in  $\text{NO}_2$ . This varies depending on the  $\text{NO}_x$  mixing ratio scenario for two reasons. First, as the  $\text{NO}_x$  mixing ratio gets bigger, the closer the  $\text{NO}_x$  gets to achieving the EIE and the bigger the split between  $\text{NO}$  and  $\text{NO}_2$   $\delta^{15}\text{N}$  values (40‰ versus 10‰ for Leighton+ $\text{O}_3$ ). Secondly, differences in the amount of  $\text{NO}_x$  result in different  $\text{NO}/\text{NO}_2$  ratios as the simulations progress. For example, under low  $\text{NO}_x$  mixing ratios the nighttime  $\text{NO}/\text{NO}_2 < .001$ , which means the  $\delta^{15}\text{N}$  value of  $\text{NO}_2$  will be close to that of total  $\text{NO}_x$ , which will be close to 0‰. At the same time the  $\delta^{15}\text{N}$  value of  $\text{NO}$  will be close to the fraction of the EIE achieved, which is about 50% under low  $\text{NO}_x$  conditions, resulting in a  $\text{NO}$   $\delta^{15}\text{N}$  of about -15‰. These two effects control the  $\delta^{15}\text{N}$  of  $\text{NO}_2$  and that in turn controls the  $\delta^{15}\text{N}$  value of  $\text{HNO}_3$ . In all scenarios the diurnal cycle repeats itself over the subsequent 4 days and a greater fraction of total  $\text{NO}$  emitted has been turned into  $\text{HNO}_3$ , so that by the end of the 5-day simulation the  $\text{HNO}_3$   $\delta^{15}\text{N}$  values converge towards 0‰, the defined value of  $\text{NO}_x$  emissions in the simulations.

The modeled  $\delta^{15}\text{N}$  values of  $\text{HONO}$  also have a diurnal pattern that can also be traced to diurnal chemistry and isotope mass balance. Similar to the photolysis and photolysis +  $\text{O}_3$  cases, the  $\text{HONO}$   $\delta^{15}\text{N}$  values mirror the oscillation of the  $\text{NO}$   $\delta^{15}\text{N}$  values (data not shown). This is a result of  $\text{HONO}$  production by the  $\text{NO} + \text{OH}$  reaction (R38). In contrast, the  $\text{HONO}$   $\delta^{15}\text{N}$  values at night remain nearly constant despite the fact that the  $\delta^{15}\text{N}$  of  $\text{NO}$  is changing dramatically. This is because the absence of  $\text{OH}$  at night halts R38 and thus  $\text{HONO}$  production ceases and the  $\delta^{15}\text{N}$  values are simply the same as the residual daytime  $\text{HONO}$  reservoir. There is a repeated minimum in  $\text{HONO}$   $\delta^{15}\text{N}$  values occurring each morning at 7:00 over the subsequent 4 days. This is a result of the fact that, unlike  $\text{HNO}_3$ ,  $\text{HONO}$  is effectively destroyed by photolysis (R4) and  $\text{OH}$  (R45). Thus,  $\text{HONO}$  does not build up in the model over the 5-day simulation, but rather mixing ratio peaks daily (30 ppb) at around 9:00 each day. This is when the  $\text{HONO}$  production – destruction rate is greatest, and its mixing ratio then decreases to a low of 2 ppt by sunset. Since the nighttime  $\text{HONO}$ , with  $\delta^{15}\text{N} \sim +5.5\text{‰}$ , only contributes about 7% ( $f = 0.07$ ) of the morning

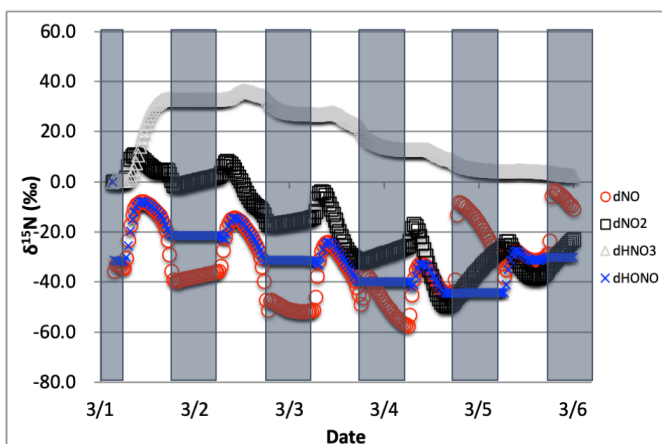


Figure 10. The time evolution of  $\delta^{15}\text{N}$  values of  $\text{NO}$ ,  $\text{NO}_2$ ,  $\text{HNO}_3$ , and  $\text{HONO}$  caused by isotope effects of Leighton reactions,  $\text{NO}_x$  isotope exchange, and  $\text{NO}_2 + \text{OH}$  reaction, with  $\text{NO}$  emission, simulation starts from Mar 1. The 5-day simulation was under the conditions list in Table S3c.

HONO spike, it does not greatly impact the control that NO  $\delta^{15}\text{N}$  has on the HONO  $\delta^{15}\text{N}$  value. This daily isotope effect should be contrasted with the HNO<sub>3</sub>  $\delta^{15}\text{N}$  trends with time. Initially HNO<sub>3</sub>  $\delta^{15}\text{N}$  values are influenced by NO<sub>2</sub>  $\delta^{15}\text{N}$  variations by NO<sub>2</sub>-OH-HNO<sub>3</sub> coupling, similar to the NO-OH-HONO coupling. But since there is no significant photochemical sink of HNO<sub>3</sub>, the control on HNO<sub>3</sub>  $\delta^{15}\text{N}$  values by HNO<sub>3</sub> accumulation increases with time, so that by day 5 the diurnal changes in NO<sub>2</sub>  $\delta^{15}\text{N}$  have almost no impact on the HNO<sub>3</sub>  $\delta^{15}\text{N}$  values (Fig. 9).

### 3.1.4 The $\delta^{15}\text{N}$ values of NO<sub>x</sub>, HONO, and HNO<sub>3</sub> due to the combined Leighton cycle, NO<sub>x</sub> isotope exchange, and NO<sub>2</sub> + OH

The effect of the NO<sub>2</sub> + OH reaction has on  $\delta^{15}\text{N}$  values of NO<sub>x</sub> and HNO<sub>3</sub> associated was then examined (Table S3c). Since R39 is the last step in HNO<sub>3</sub> production, the instantaneous  $\delta^{15}\text{N}$  HNO<sub>3</sub> =  $\delta^{15}\text{N}(\text{NO}_2) + \epsilon_{39}$ , thus the  $\delta^{15}\text{N}$  HNO<sub>3</sub> is initially 40‰ higher than the NO<sub>2</sub> (Fig. 10). This in turn depletes <sup>15</sup>N in the residual NO<sub>2</sub> leading to more negative  $\delta^{15}\text{N}$  values in NO<sub>2</sub> relative to the Leighton + exchange simulations (Fig. 10). These latter two effects are still in play as evident by the diurnal NO<sub>x</sub>  $\delta^{15}\text{N}$  cycling and  $\Delta\delta^{15}\text{N}_{\text{NO-NO}_2}$ . As the 5-day simulation progresses, the HNO<sub>3</sub>  $\delta^{15}\text{N}$  value approaches 0‰, approaching the  $\delta^{15}\text{N}$  of NO emissions, as expected based on isotope mass balance. We point out that this convergence to the source NO<sub>x</sub>  $\delta^{15}\text{N}$  value is much slower in this case than the Leighton and exchanges cases. This highlights the importance of the knowing the correct  $\epsilon_{48}$ . If  $\epsilon_{39} \sim 0$  as suggested by Freyer (1991) then daytime the  $\delta^{15}\text{N}$  HNO<sub>3</sub>  $\cong$   $\delta^{15}\text{N}$  NO<sub>2</sub>, demonstrably lower than the  $\epsilon_{39} \sim 40$ ‰ case. In the end the average daytime  $\delta^{15}\text{N}$  value of HNO<sub>3</sub> for the entire simulation is about 10‰ higher than the  $\delta^{15}\text{N}$  of the NO<sub>x</sub> source (here defined as 0‰).

### 3.2 The $\delta^{15}\text{N}$ values of NO<sub>x</sub>, HONO, and HNO<sub>3</sub> due to nighttime chemistry

The role that nighttime chemistry plays in determining the  $\delta^{15}\text{N}$  values of NO<sub>x</sub>, HONO, and HNO<sub>3</sub> was investigated by iteratively adding relevant fractionation factors to iRACM. The nighttime chemistry effect was assessed by separating the effects of NO<sub>3</sub> radical chemistry and N<sub>2</sub>O<sub>5</sub> heterogeneous hydrolysis. NO<sub>3</sub> radical chemistry is only relevant at night because of its short daytime lifetime with respect to photolysis, which keeps its daytime mixing ratios at the sub ppt<sub>v</sub> levels [Platt *et al.*, 1984]. At night NO<sub>3</sub> builds up and produces HNO<sub>3</sub> [Aldener *et al.*, 2006; Finlayson-Pitts and Pitts, 1997; Horowitz *et al.*, 1998] via reactions with hydrocarbons (R91-97). The magnitude of this isotope effect was tested by adding NO<sub>3</sub> the isotope fractionation factors for R91-97 (see methods) and altering VOC emission rates to simulate clean, moderate, and extreme VOC pollution environments. Likewise, N<sub>2</sub>O<sub>5</sub> only

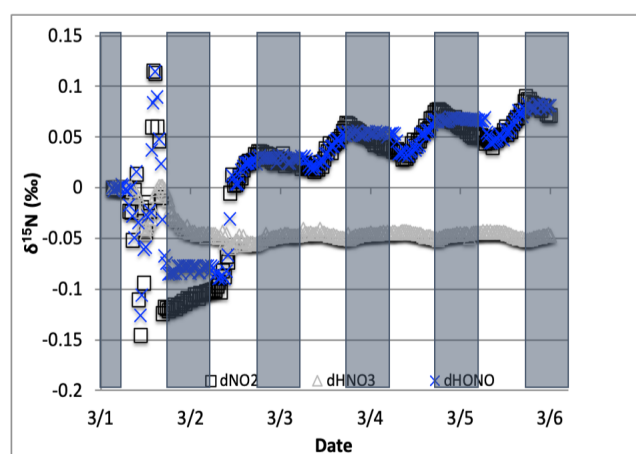


Figure 11. The difference between the  $\delta^{15}\text{N}$  values of NO<sub>2</sub>, HONO, and HNO<sub>3</sub> when NO<sub>3</sub> + VOC  $\rightarrow$  HNO<sub>3</sub> reactions are included and excluded (NO was omitted for clarity). The 5-day simulation was under the conditions list in Table S3e. Total VOC mixing ratios during the last day of the March 1 simulation was 550-670 ppb C.

accumulates at night when it begins producing  $\text{HNO}_3$  on aerosol surfaces [Chang *et al.*, 2011]. The magnitude of this isotope effect was tested by adding the  $\text{N}_2\text{O}_5$  EIE (see methods) and adding the first order  $\text{N}_2\text{O}_5$  heterogeneous pathway (see methods) to  $i_{\text{N}}\text{RACM}$ . The first-order rate constant was adjusted to simulate clean, polluted, and extreme pollution environments where aerosol surface area density largely controls the rate constant [Riemer *et al.*, 2003 Chang *et al.*, 2011].

### 3.2.1 The $\delta^{15}\text{N}$ values of $\text{NO}_x$ , HONO, and $\text{HNO}_3$ due to $\text{NO}_3 + \text{VOC}$ reactions

The effect on the  $\delta^{15}\text{N}$  values of  $\text{NO}_x$ ,  $\text{HNO}_3$ , HONO associated with the KIE occurring during  $\text{NO}_3 + \text{VOC}$  nighttime reactions (R91-R97) were first examined. Four simulations were run that included the isotope effects ( $\alpha$  values in Table S4) of the Leighton cycle (R1 and R48),  $\text{NO}_x$  isotope exchange (R238),  $\text{NO}_2 + \text{OH}$  production of  $\text{HNO}_3$  (R39), and the KIE effects (R91-R97), as well as  $\text{NO}$  emissions. The simulation tested first was the March test case (medium VOC  $\sim 360$  ppbv). Then, two simulations were run for June 1 (extended sunlight, warm temperatures), one with high initial of VOC concentrations and a high VOC emission rate ( $2 \text{ ppbv h}^{-1}$ ) and one with low emission rate of VOCs ( $0.4 \text{ ppbv h}^{-1}$ ). The same two initial conditions were used in the Jan. 1 test case to assess if the extended nighttime and cold temperatures significantly affected the  $\text{NO}_x$  of  $\text{HNO}_3$   $\delta^{15}\text{N}$  values produced by  $\text{NO}_3$  radicals. The impact of  $\text{NO}_3$  reactions on  $\text{NO}_y$   $\delta^{15}\text{N}$  values was determined by subtracting these simulated  $\delta^{15}\text{N}$  values from those same simulations when only the Leighton cycle, exchange and  $\text{OH} + \text{NO}_2$  reaction was considered (Section 3.1).

The  $\text{NO}_3 + \text{VOC}$  KIE induced a minor diurnal pattern on the  $\delta^{15}\text{N}$  values of  $\text{NO}_x$ , and HONO, and a trend for  $\text{HNO}_3$  for the March test case, but the size of the effect was relatively small (e.g.,  $< 0.4\text{‰}$ ; Fig. 11). At the start of the simulation (3 am) there is no  $\text{HNO}_3$ , therefore the initial  $\text{HNO}_3$  is produced via  $\text{OH} + \text{NO}_2$  reaction (R39),

$\delta^{15}\text{N}$  values of  $\text{HNO}_3$  decreased from 0.35 to 0.2‰ during the night. The pattern is because of increasing the importance of R91-R97 in  $\text{HNO}_3$  production at night. The smallness of the effect is because  $\alpha$  values are all relatively small, the average  $\delta$  for the  $\text{NO}_3 + \text{VOC}$  is about  $-4\text{‰}$ , and the relatively small amount of  $\text{HNO}_3$  produced via these pathways (around 2.6 % of 24-hour  $\text{HNO}_3$ ). The first source of the  $\text{HNO}_3$  in the simulation (3 to 6 am) is the  $\text{NO}_3 + \text{VOC}$  reactions and results in a slight negative  $\delta^{15}\text{N}$  in  $\text{HNO}_3$  value ( $-0.01\text{‰}$ ). This leaves the residual  $\text{NO}_3^-$   $^{15}\text{N}$  enriched that is then photolyzed into  $\text{NO}_2$  at sunrise and used  $\text{NO}_2 + \text{OH} \rightarrow \text{HNO}_3$  production resulting in slight positive  $\delta^{15}\text{N}$  values ( $+0.35\text{‰}$ ) (Fig. 11). The range of the diurnal  $\text{HNO}_3$   $\delta^{15}\text{N}$  oscillation dampens as the fraction of emitted  $\text{NO}$  that has been converted to  $\text{HNO}_3$  has increased over time. The diurnal and multiday change in  $\delta^{15}\text{N}$  of  $\text{HNO}_3$  changes did not significantly change during the winter and summer simulations (Fig. 12) run with and without the KIE for R91-R97

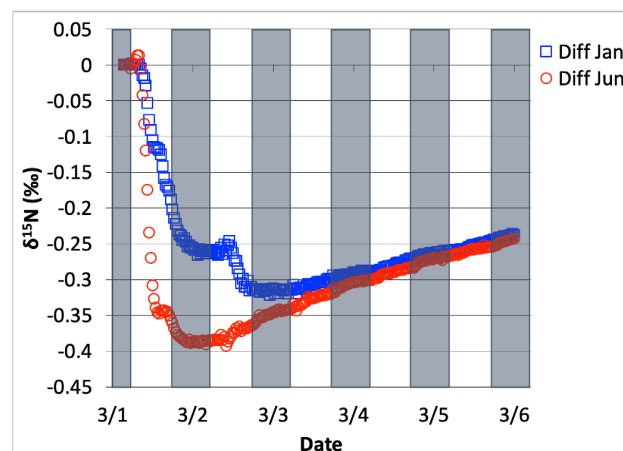


Figure 12. The difference in  $\delta^{15}\text{N}(\text{HNO}_3)$  values when  $\text{NO}_3 + \text{VOC} \rightarrow \text{HNO}_3$  reactions are included and excluded, for Mar 1 simulation, relative to Jun 1 simulation ( $\square$ ) and Jan 1 simulation ( $\circ$ ). The 5-day simulation was under the conditions list in Table S3e.

show negligible differences, similar to those in Fig. 11. In conclusion, although there is some  $\delta^{15}\text{N}$  effect associated with  $\text{NO}_3 + \text{VOC}$  chemistry, it is much smaller than the effects associated with the Leighton cycle,  $\text{NO}_2 + \text{OH}$ , and  $\text{NO}_x$  equilibrium.

### 3.2.2 The $\delta^{15}\text{N}$ values of $\text{NO}_x$ , HONO, and $\text{HNO}_3$ due to $\text{N}_2\text{O}_5$ reactions

The effect on the  $\delta^{15}\text{N}$  values of  $\text{NO}_x$ ,  $\text{HNO}_3$ , HONO associated with the EIE of  $\text{N}_2\text{O}_5$  heterogeneous hydrolysis was also tested. March 1 simulations with N emissions and  $k_{\text{N}_2\text{O}_5} = 0.1 \text{ s}^{-1}$  were run that included the isotope effects of the Leighton cycle (R1 and R48),  $\text{NO}_x$  isotope exchange (R238), OH production of  $\text{HNO}_3$  (R39), and the  $\text{N}_2\text{O}_5$  EIE (R53-54) KIE (R239) (Table S5), as well as NO emissions. These simulations were compared to an identical simulation but where the  $\alpha_{\text{N}_2\text{O}_5}$  was set equal to 1.0. This ensured that the  $\text{NO}_y$  chemistry was not altered when comparing the two simulations (i.e.,  $\alpha_{\text{N}_2\text{O}_5} = 1.029$  vs.  $\alpha_{\text{N}_2\text{O}_5} = 1.0$ ). The effect of  $\text{N}_2\text{O}_5$  chemistry on the  $\delta^{15}\text{N}$  values of  $\text{NO}_2$  and  $\text{HNO}_3$  was investigated. Similar to the March 1  $\text{NO}_3 + \text{VOC}$  tests, simulations with R1, R39, R48, R238, and R239 isotope effects active were run and then compared to simulations with the same conditions but with R239 turned off. In addition, March simulations were run using three different  $k_{\text{N}_2\text{O}_5}$  values (.01, 0.1 and 1) and compared to each other in order to test the range of  $\text{NO}_2$  and  $\text{HNO}_3$   $\delta^{15}\text{N}$  values that could be generated solely by heterogeneous  $\text{N}_2\text{O}_5$  hydrolysis.

The average daily  $\delta^{15}\text{N}$  values of  $\text{HNO}_3$  exhibit some diurnal oscillations that roughly reach a steady state average value after simulation day 2. At that point  $\text{HNO}_3$  has a  $\delta^{15}\text{N} = +2.5\text{‰}$  relative to the  $\alpha_{\text{N}_2\text{O}_5} = 1.0$  simulation. In contrast the  $\text{NO}_2$   $\delta^{15}\text{N}$  values oscillate diurnally by about  $\pm 2\text{‰}$  around an average daily difference of about  $-8\text{‰}$ . This change is due to the R53-54 equilibrium, which predicts  $^{15}\text{N}$  enrichment in  $\text{N}_2\text{O}_5$  (and thus  $\text{HNO}_3$ ) and depletion in  $\text{NO}_3$  and  $\text{NO}_2$ . The  $\text{N}_2\text{O}_5$  produces  $\text{HNO}_3$  with the highest  $\delta^{15}\text{N}$  difference ( $\sim +29\text{‰}$ ) during the first simulation morning. This is because all of the initial  $\text{HNO}_3$  is produced by  $\text{N}_2\text{O}_5$  due to the 3 am simulation start time. The roughly steady state  $\text{HNO}_3$   $\delta^{15}\text{N}$  value of  $+2.5\text{‰}$  is a consequence of the fact that when  $\alpha_{\text{N}_2\text{O}_5} = 1.0$   $\text{HNO}_3$  is being produced by  $\text{N}_2\text{O}_5$  at  $0\text{‰}$  and when  $\alpha_{\text{N}_2\text{O}_5} = 1.029$  it is being produced at  $+29\text{‰}$ . The ratio of this simulated  $+2.5\text{‰}$  value and  $\text{N}_2\text{O}_5$  enrichment factor of  $+29\text{‰}$  yields 0.086, the fraction of  $\text{HNO}_3$  produced by  $\text{N}_2\text{O}_5$ . This is similar to the fraction of  $\text{HNO}_3$  produced in simulations when the  $\text{N}_2\text{O}_5$  reaction was active and where it is inactive, which yielded a fraction of 0.064. The difference in these fractions is because deactivating  $\text{N}_2\text{O}_5$  chemistry changes overall  $\text{NO}_y$  chemistry and  $\text{HNO}_3$  production [Dentener and Crutzen, 1990].

The effect of  $\text{N}_2\text{O}_5$  chemistry on the  $\delta^{15}\text{N}$  values of  $\text{NO}_2$  is more dynamic than  $\text{HNO}_3$  (Fig. 13). This is mainly due to the fact that  $\text{HNO}_3$  is continually building up over time and thus its

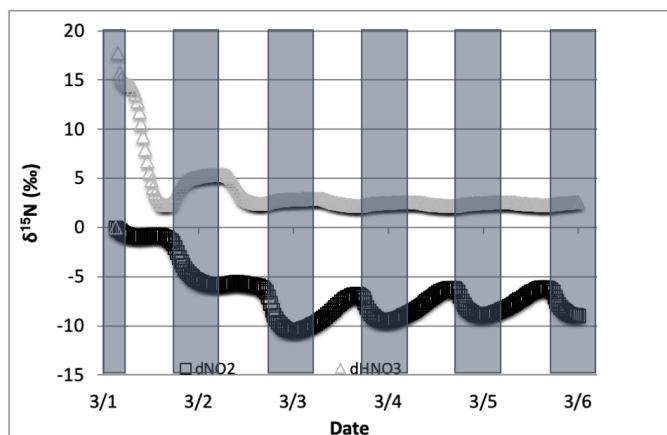


Figure 13. The difference in  $\delta^{15}\text{N}$  values of  $\text{NO}_2$  and  $\text{HNO}_3$  when the isotopic effect during  $\text{N}_2\text{O}_5$  heterogeneous reactions (R53-54, R239) is included ( $\alpha_{\text{N}_2\text{O}_5} = 1.029$ ) and when it is excluded ( $\alpha_{\text{N}_2\text{O}_5} = 1.0$ ). The 5-day simulation was under the conditions list in Table S3e.



$\delta^{15}\text{N}$  is less susceptible to change by small additions. The oscillation in the  $\text{NO}_2$   $\delta^{15}\text{N}$  value becomes more negative at night, which corresponds to the increase in the  $\text{HNO}_3$   $\delta^{15}\text{N}$  values. This is a reflection of  $^{15}\text{N}$  preferentially incorporating into  $\text{N}_2\text{O}_5$  resulting in  $\text{NO}_2$  depleted in  $^{15}\text{N}$ . Similar oscillations are found in  $\text{NO}$  and  $\text{HONO}$  (data not shown) as they are connected to  $\text{NO}_2$  build-up and decay diurnally. This suggests that night-time partitioning of  $\text{NO}_y$  will have a small but measurable influence on daytime  $\text{NO}_y$   $\delta^{15}\text{N}$  values. The effect of using different  $k_{\text{N}_2\text{O}_5}$  values had a small but measurable effect on the  $\text{NO}_2$  and  $\text{HNO}_3$   $\delta^{15}\text{N}$  values. Simulations that used a  $k_{\text{N}_2\text{O}_5} = 1.0$  resulted in  $\text{HNO}_3$   $\delta^{15}\text{N}$  values that were about 2‰ lower than those run at  $k_{\text{N}_2\text{O}_5} = 0.01$  and 1‰ heavier than when  $k_{\text{N}_2\text{O}_5} = 1.0$ . This makes sense because the mean EIE for  $\text{N}_2\text{O}_5$  (29‰) is lower than that for  $\text{NO}_2 + \text{OH}$  (40‰), therefore as  $\text{N}_2\text{O}_5$  produces more  $\text{HNO}_3$  its  $\delta^{15}\text{N}$  value would decrease with respect to that of daytime  $\text{HNO}_3$  production. Thus, the model predicts lower  $\text{HNO}_3$   $\delta^{15}\text{N}$  values in cold, dark polluted regions (relative to the tropics where) where  $\text{N}_2\text{O}_5$  heterogeneous hydrolysis may be the main  $\text{HNO}_3$  production pathway [Dentener and Crutzen, 1990].

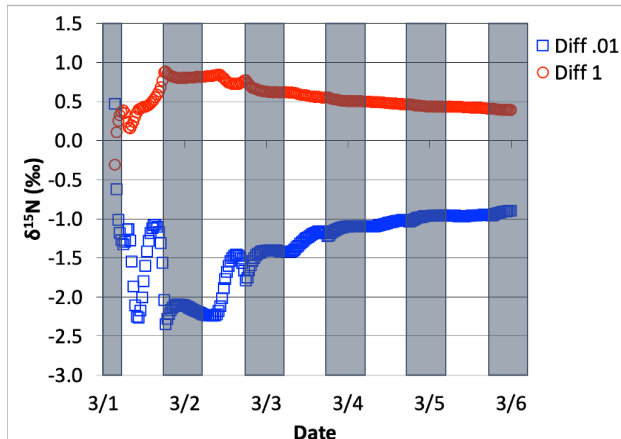


Figure 14. The difference in  $\delta^{15}\text{N}(\text{HNO}_3)$  values when the isotopic effect during  $\text{N}_2\text{O}_5$  heterogeneous reactions is included and when it is excluded, for the simulation of  $k_{\text{N}_2\text{O}_5} = 0.1$ , relative to 0.01 ( $\square$ ) and 1.0 ( $\circ$ ). The 5-day simulation was under the conditions list in Table S3e.

### 3.3 Assessing $i_{\text{N}}\text{RACM}$ 's ability to predict in particulate $\text{NO}_3^-$

There are a number of challenges when trying to compare the  $i_{\text{N}}\text{RACM}$  model predictions of  $\text{NO}_y$   $\delta^{15}\text{N}$  values with observations in real world. First, there has yet to be a study where the  $\delta^{15}\text{N}$  values of  $\text{NO}$ ,  $\text{NO}_2$ , and  $\text{NO}_3^-$  have been simultaneously measured. The most abundant data is on the  $\delta^{15}\text{N}$  value of  $\text{NO}_3^-$  in aerosols or rainwater. Even with these studies, a direct comparison is difficult because of the  $\delta^{15}\text{N}$  value of the source  $\text{NO}_x$  may be variable in space and time. The  $\delta^{15}\text{N}$  value of  $\text{NO}_x$  sources can range from -40 to +20 ‰ and both  $\text{NO}_x$  sources and  $\text{NO}_3^-$  deposition will be a strong function of the transport history of the air mass that is sampled. Without a 3-D chemical transport model that includes the  $i_{\text{N}}\text{RACM}$  mechanism, a direct comparison with most  $\text{NO}_3^-$   $\delta^{15}\text{N}$  studies would be tenuous. In addition, most  $\text{NO}_y$   $\delta^{15}\text{N}$  studies provide neither trace gas concentrations ( $\text{NO}_x$ ,  $\text{O}_3$ ,  $\text{CO}$ ,  $\text{VOC}$ ) nor local trace gas emissions that would be required to constrain  $i_{\text{N}}\text{RACM}$  for it make an accurate prediction of secondary pollutants or  $\delta^{15}\text{N}$  values.

The most complete dataset for which to evaluate the  $i_{\text{N}}\text{RACM}$  mechanism is from Riha [2013] in a study in Tucson AZ, USA. In that study  $\text{PM}_{2.5}$  and  $\text{PM}_{10}$  were collected weekly (24-hour period) for one year (2006) and the  $\delta^{15}\text{N}$  value of water soluble  $\text{NO}_3^-$  from was determined (Fig. 15). It contains  $\text{PM}$  mass and  $\text{NO}_3^-$   $\delta^{15}\text{N}$  and concentration data, local measurements of the main trace gases (except  $\text{VOCs}$ ) and meteorology (temperature, relative humidity, wind) were available. In addition, detailed local primary pollutant emission inventories have been developed [Diem and Comrie, 2001]. Tucson is a city with little industry or power generation so roughly 80% of the  $\text{NO}_x$  is due to vehicles and the relative proportion of all  $\text{NO}_x$  sources is invariant throughout the year (Fig. S1). Further, Tucson is surrounded by a desert landscape and by and

large not influences by regional pollution sources outside the city.  $i_N$ RACM was initialized with observed trace gas concentrations and  $\text{NO}_x$  and VOC emissions were based on previous work [Riha, 2013] and the source  $\text{NO}_x$   $\delta^{15}\text{N}$  value was set to  $-3\text{‰}$ , typical of vehicle emissions [Walters et al., 2015] and run for 1 week from the first day of each month. The aerosol surface area used to calculate  $k_{\text{N}_2\text{O}_5}$  was based on monthly average PM mass (Fig. S2).

The predicted  $\text{NO}_3^-$  (as  $\text{HNO}_3$ )  $\delta^{15}\text{N}$  values (After  $36 \pm 12$  hours) matched remarkably well with the observed  $\delta^{15}\text{N}$  values in  $\text{PM}_{2.5}$  and  $\text{PM}_{10}$  (Fig. 15). Observed maximums were in the winter months, peaking January at  $15\text{‰}$  close to the model maximum in January of  $17\text{‰}$ . The minimum  $\delta^{15}\text{N}$  values ( $-2\text{‰}$ ) are measured in July, similar to model predictions of  $0\text{‰}$  during July. The model captures the seasonal trend quite well, including the Spring plateau.

This suggests that at this location, the observed seasonal variation in  $\text{PM NO}_3^- \delta^{15}\text{N}$  values can be explained isotope effects associated with the photochemical conversion of  $\text{NO}_x$  into  $\text{HNO}_3$ . The wider range in  $\text{HNO}_3 \delta^{15}\text{N}$  values in the winter months relative to summer months is due to difference in sunlight and oxidant loads. In winter sunlight hours are at a minimum (8.5 hours versus 12.8 in June) and ozone mixing ratios are a factor of 4-5 lower compared to the summer months [Riha, 2013]. This results in rapid conversion of  $\text{NO}_x$  into  $\text{HNO}_3$  in the summer the  $\text{HNO}_3/(\text{HNO}_3+\text{NO}_x)$  exceeds 0.90 within two days whereas it requires six days during the winter (Fig. S3). The result is that in the summer  $\text{HNO}_3 \delta^{15}\text{N}$  values rapidly approach the  $\delta^{15}\text{N}$  of the  $\text{NO}_x$  source, whereas in the winter there is greater diurnal and daily variability until the very end of the simulation. The rapid swings in  $\text{HNO}_3 \delta^{15}\text{N}$  values are thus a function of the chemical lifetime of  $\text{NO}_x$  and physical lifetime of  $\text{HNO}_3$  with respect to wet (and dry) deposition. Thus, when the atmosphere is cleansed by regional rainfall, the isotope effects associated with photochemical oxidation will have a greater influence relative to  $\text{NO}_x$  sources and this is a plausible explanation of rapid changes in the  $\delta^{15}\text{N}$  of rain nitrate over the course of a storm [Rose et al., 2019]. Analysis of hourly  $\text{HNO}_3$  production revealed that  $\sim 80\%$  of  $\text{HNO}_3$  is produced in the daytime, mainly by the  $\text{NO}_2 + \text{OH}$  reaction and  $20\%$  is produced during the night ( $\text{N}_2\text{O}_5$  heterogenous hydrolysis). The model reproduces  $\text{O}_3$  and  $\text{NO}_x$  concentrations rather accurately (Fig S2) but  $\text{HNO}_3$  concentrations that are about 10 times the  $\text{PM NO}_3^-$  concentration. This is not surprising because the 0-D models do not account for  $\text{HNO}_3$  deposition, its dilution as it mixes into to the top of the boundary layer, or partitioning between aerosol and the gas phase. Indeed, seasonal differences in boundary layer height alone can dilute by a factor of 5 or higher [Riha, 2013].

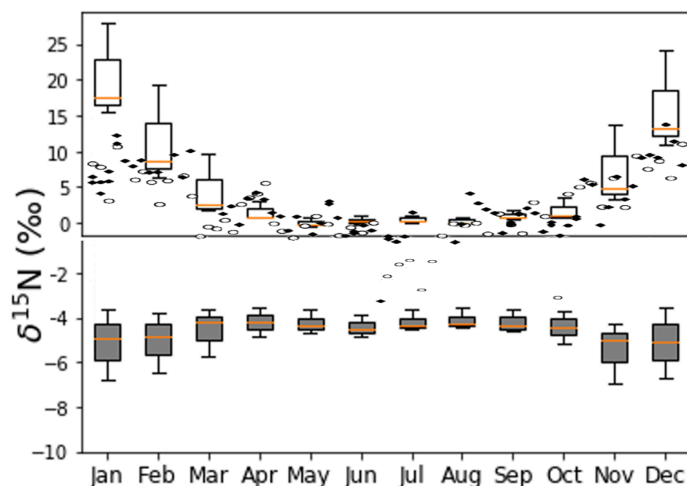


Figure 15. Upper panel is the observed  $\text{NO}_3^- \delta^{15}\text{N}$  values of PM in the city of Tucson (Riha, 2013) and box and whisker plots values predicted by  $i_N$ RACM (1 week simulation, Red line = median, box = 1st and 3rd quantile, whisker is minimum and maximum). The bottom box and whisker plots are for  $i_N$ RACM simulations with  $R39 \alpha = 0.9971$  from Freyer (1991).

## 4. Conclusion

We have developed the first 0-D photochemical box model for  $^{15}\text{N}$  compounds in the tropospheric  $\text{NO}_x\text{-NO}_y$  cycle. It was shown that of the 100's of N reactions in the RACM mechanism only a handful significantly impact the  $\delta^{15}\text{N}$  of the main  $\text{NO}_y$  compounds ( $\text{NO}_x$ , HONO,  $\text{HNO}_3$ ). Primarily these reactions are Leighton cycle reactions,  $\text{NO}_2 + \text{OH}$ , and  $\text{NO}_x$  isotope exchange, with  $\text{N}_2\text{O}_5$  and nitrate radical reactions having a significant, but minor influence on  $\text{NO}_y$   $\delta^{15}\text{N}$  values. The model accuracy and its validation could be improved with additional research. The  $i_{\text{N}}\text{RACM}$  model could be refined by additional theoretical and/or experimental determination of the isotope fractionation factors for the N reactions. First and foremost, the fractionation factor for the  $\text{NO}_2 + \text{OH}$  reaction needs evaluating in a more robust manner. Likewise, the fractionation factor for the  $\text{NO} + \text{OH}$ , another 3-body reaction, will have a large influence on HONO  $\delta^{15}\text{N}$  values and determining its value will be key for interesting future HONO  $\delta^{15}\text{N}$  data. The fractionation factor for  $\text{NO}_2$  photolysis requires attention given the limitation of the  $\Delta\text{ZPE}$  PHIFE model [Blake et al., 2003; Liang et al., 2004; Miller and Yung, 2000]. On the validation end, the simultaneous measurement of  $\delta^{15}\text{N}$  in multiple  $\text{NO}_y$  compounds would expose the accuracy or limitations of the  $i_{\text{N}}\text{RACM}$  model in a quantitative way. The  $i_{\text{N}}\text{RACM}$  model reproduced observed  $\delta^{15}\text{N}$  data from year-long study on the isotopic composition of particulate nitrate collected in Tucson AZ. This suggests that the model, which is publicly available, could be used as an analytical tool for researchers using  $^{15}\text{N}$  to gain insight into  $\text{NO}_x$  sources and transformation chemistry.

The  $i_{\text{N}}\text{RACM}$  model is the first step in our development of N isotope enabled 3-D chemical transport model ( $i_{\text{N}}\text{CMAQ}$ ). That model will couple  $i_{\text{N}}\text{RACM}$  with a  $^{15}\text{NO}_x$  emissions model ( $i_{\text{N}}\text{NEI}$ ) and WRF generated transport. The  $i_{\text{N}}\text{RACM}$  results show that photochemistry is an important control on the  $\delta^{15}\text{N}$  of the  $\text{NO}_y$  compounds, in particular  $\text{NO}_3^-$ , for which there is a large and growing data set that can be used to validate the model. This is important because this suggests that  $\delta^{15}\text{N}$  in  $\text{NO}_y$  compounds could be used as a validation of different photochemical mechanisms. Further, if the photochemical effect can be deconvoluted from the observations then observed  $\text{NO}_y$   $\delta^{15}\text{N}$  could be used as a constraint and validation of  $\text{NO}_x$  emissions inventories. Expanded to the global scale, such a model could potentially be used to investigate the cause of  $\delta^{15}\text{N}$  versions in  $\text{NO}_3^-$  found in Antarctic and Greenland ice cores (Hastings et al., 2009) and linked to historical changes in  $\text{NO}_x$  emission and  $\text{NO}_y$  chemistry.

**Code availability:** Fortran code and associated input files are archived on Zenodo.org (10.5281/zenodo.3834914) An online version of this  $i_{\text{N}}\text{RACM}$  model is available for public use at <https://mygeohub.org/tools/sbox/>

**Author contribution:** Greg Michalski was the lead investigator for the project designed the modeling experiments, organized the tasks, and wrote the manuscript. Huan Fang and David Mase modified the RACM code to include  $^{15}\text{N}$  isotopes, assisted in writing and editing the manuscript. Wendell W Walters derived EIE, KIE, and PHIFE used in the model and assisted in writing and editing the paper

**Acknowledgements:** We would like to thank the Purdue Research Foundation and the Purdue Climate Change Research Center for providing funding for the project. We would like to thank Bo Sun for helping with the FORTRAN coding and data generation.

The authors declare that they have no conflict of interest.

## References

- Aldener, M., Brown, S. S., Stark, H., Williams, E. J., Lerner, B. M., Kuster, W. C., ... & Ravishankara, A. R. (2006). Reactivity and loss mechanisms of  $\text{NO}_3$  and  $\text{N}_2\text{O}_5$  in a polluted marine environment: Results from in situ measurements during New England Air Quality Study 2002. *Journal of Geophysical Research: Atmospheres*, *111*(D23).
- Andreae, M. O., and P. J. Crutzen (1997), Atmospheric aerosols: biogeochemical sources and role in atmospheric chemistry, *Science*, *276*(5315), 1052-1058.
- Anttila, T., Kiendler-Scharr, A., Tillmann, R., & Mentel, T. F. (2006). On the reactive uptake of gaseous compounds by organic-coated aqueous aerosols: Theoretical analysis and application to the heterogeneous hydrolysis of  $\text{N}_2\text{O}_5$ . *The Journal of Physical Chemistry A*, *110*(35), 10435-10443.
- Atkinson, R. (1990), Gas-phase tropospheric chemistry of organic-compounds - a review, *Atmospheric Environment Part a-General Topics*, *24*(1), 1-41, doi:10.1016/0960-1686(90)90438-s.
- Atkinson, R. (2000), Atmospheric chemistry of VOCs and  $\text{NO}_x$ , *Atmospheric Environment*, *34*(12-14), 2063-2101.
- Atkinson, R., D. L. Baulch, R. A. Cox, R. F. Hampson, J. A. Kerr, and J. Troe (1992), Evaluated kinetic and photochemical data for atmospheric chemistry supplement-iv - IUPAC subcommittee on gas kinetic data evaluation for atmospheric chemistry, *Journal of Physical and Chemical Reference Data*, *21*(6), 1125-1568, doi:10.1063/1.555918.
- Bauer, S. E., D. Koch, N. Unger, S. M. Metzger, D. T. Shindell, and D. G. Streets (2007), Nitrate aerosols today and in 2030: a global simulation including aerosols and tropospheric ozone, *Atmospheric Chemistry and Physics*, *7*(19), 5043-5059
- Bertram, T. H., & Thornton, J. A. (2009). Toward a general parameterization of  $\text{N}_2\text{O}_5$  reactivity on aqueous particles: the competing effects of particle liquid water, nitrate and chloride. *Atmospheric Chemistry and Physics*, *9*(21), 8351-8363.
- Bigeleisen, J. (1958), Second-Order Sum Rule for the Vibrations of Isotopic Molecules and the Second Rule of the Mean, *The Journal of Chemical Physics*, *28*(4), 694-699.
- Bigeleisen, J., and M. G. Mayer (1947), Calculation of Equilibrium Constants for Isotopic Exchange Reactions, *The Journal of Chemical Physics*, *15*(5), 261-267.
- Bigeleisen, J., and M. Wolfsberg (1958), Theoretical and experimental aspects of isotope effects in chemical kinetics, *Advances in Chem. Phys. (Prigogine, I. Interscience Publishers, Inc. , New York)*, *1*, 15-76.
- Blake, G. A., M. C. Liang, C. G. Morgan, and Y. L. Yung (2003), A born-oppenheimer photolysis model of  $\text{N}_2\text{O}$  fractionation, *Geophysical Research Letters*, *30*(12), 58/51-58/54.

Bloss, W. J., M. J. Evans, J. D. Lee, R. Sommariva, D. E. Heard, and M. J. Pilling (2005), The oxidative capacity of the troposphere: Coupling of field measurements of OH and a global chemistry transport model, *Faraday Discussions*, 130, 425-436.

Brimblecombe, P., H. Hara, and D. Houle (2007), *Acid Rain - Deposition to Recovery*, Springer.

Brown, S. S., J. B. Burkholder, R. K. Talukdar, and A. R. Ravishankara (2001), Reaction of hydroxyl radical with nitric acid: insights into its mechanism, *Journal of Physical Chemistry A*, 105(9), 1605-1614.

Brown, L. L., & Begun, G. M. (1959). Nitrogen isotopic fractionation between nitric acid and the oxides of nitrogen. *The Journal of Chemical Physics*, 30(5), 1206-1209.

Brown, S. S., et al. (2006), Variability in nocturnal nitrogen oxide processing and its role in regional air quality, *Science*, 311(5757), 67-70.

Bruningfann, C. S., and J. B. Kaneene (1993), The Effects of Nitrate, Nitrite and N-Nitroso Compounds on Human Health - A Review, *Veterinary and Human Toxicology*, 35(6), 521-538.

Cao, Z. Y., X. H. Zhou, Y. J. Ma, L. P. Wang, R. D. Wu, B. Chen, and W. X. Wang (2017), The Concentrations, Formations, Relationships and Modeling of Sulfate, Nitrate and Ammonium (SNA) Aerosols over China, *Aerosol and Air Quality Research*, 17(1), 84-97, doi:10.4209/aaqr.2016.01.0020.

Chai, J. J., and M. G. Hastings (2018), Collection Method for Isotopic Analysis of Gaseous Nitrous Acid, *Analytical Chemistry*, 90(1), 830-838, doi:10.1021/acs.analchem.7b03561.

Chang, W. L., P. V. Bhave, S. S. Brown, N. Riemer, J. Stutz, and D. Dabdub (2011), Heterogeneous Atmospheric Chemistry, Ambient Measurements, and Model Calculations of N<sub>2</sub>O<sub>5</sub>: A Review, *Aerosol Science and Technology*, 45(6), 665-695.

Charlson, R. J., S. E. Schwartz, J. M. Hales, R. D. Cess, J. A. Coakley, J. E. Hansen, and D. J. Hofmann (1992), Climate Forcing by Anthropogenic Aerosols, *Science*, 255(5043), 423-430.

Chen, W. T., H. Liao, and J. H. Seinfeld (2007), Future climate impacts of direct radiative forcing of anthropogenic aerosols, tropospheric ozone, and long-lived greenhouse gases, *Journal of Geophysical Research-Atmospheres*, 112(D14).

Davis, J. M., Bhave, P. V., & Foley, K. M. (2008). Parameterization of N<sub>2</sub>O<sub>5</sub> reaction probabilities on the surface of particles containing ammonium, sulfate, and nitrate. *Atmospheric Chemistry and Physics*, 8(17), 5295-5311.

Day, D. A., M. B. Dillon, P. J. Wooldridge, J. A. Thornton, R. S. Rosen, E. C. Wood, and R. C. Cohen (2003), On alkyl nitrates, O<sub>3</sub>, and the "missing NO<sub>y</sub>", *Journal of Geophysical Research-Atmospheres*, 108(D16), doi:10.1029/2003jd003685.

DeMore, W. B., S. P. Sander, D. M. Golden, R. F. Hampson, M. J. Kurylo, C. J. Howard, A. R. Ravishankara, C. E. Kolb, and M. J. Molina, (1994), Chemical kinetics and photochemical data for use in stratospheric modeling, Eval. 11, *Natl. Aeronaut. and Space Admin., Jet Propul. Lab.*

Dentener, F. J., and P. J. Crutzen (1993), Reaction of nitrogen pentoxide on tropospheric aerosols: Impact on the global distributions of NO<sub>x</sub>, ozone, and hydroxyl, *Journal of Geophysical Research*, 98(D4), 7149-7163.

Diem, J. E., & Comrie, A. C. (2001). Allocating anthropogenic pollutant emissions over space: application to ozone pollution management. *Journal of environmental management*, 63(4), 425-447.

Du, E. Z., M. E. Fenn, W. De Vries, and Y. S. Ok (2019), Atmospheric nitrogen deposition to global forests: Status, impacts and management options, *Environmental Pollution*, 250, 1044-1048, doi:10.1016/j.envpol.2019.04.014.

Elliott, E. M., C. Kendall, E. W. Boyer, D. A. Burns, G. G. Lear, H. E. Golden, K. Harlin, A. Bytnerowicz, T. J. Butler, and R. Glatz (2009), Dual nitrate isotopes in dry deposition: Utility for partitioning NO<sub>x</sub> source contributions to landscape nitrogen deposition, *Journal of Geophysical Research-Biogeosciences*, 114.

Elliott, E. M., C. Kendall, S. D. Wankel, D. A. Burns, E. W. Boyer, K. Harlin, D. J. Bain, and T. J. Butler (2007), Nitrogen isotopes as indicators of NO<sub>x</sub> source contributions to atmospheric nitrate deposition across the Midwestern and northeastern United States, *Environmental Science & Technology*, 41(22), 7661-7667.

Elliott, E. M., Z. J. Yu, A. S. Cole, and J. G. Coughlin (2019), Isotopic advances in understanding reactive nitrogen deposition and atmospheric processing, *Science of the Total Environment*, 662, 393-403, doi:10.1016/j.scitotenv.2018.12.177.

Felix, J. D., and E. M. Elliott (2014), Isotopic composition of passively collected nitrogen dioxide emissions: Vehicle, soil and livestock source signatures, *Atmospheric Environment*, 92, 359-366, doi:10.1016/j.atmosenv.2014.04.005.

Felix, J. D., E. M. Elliott, and S. L. Shaw (2012), Nitrogen Isotopic Composition of Coal-Fired Power Plant NO<sub>x</sub>: Influence of Emission Controls and Implications for Global Emission Inventories, *Environmental Science & Technology*, 46(6), 3528-3535.

Felix, J. D., Elliott, E. M., Avery, G. B., Kieber, R. J., Mead, R. N., Willey, J. D., & Mullaugh, K. M. (2015). Isotopic composition of nitrate in sequential Hurricane Irene precipitation samples: implications for changing NO<sub>x</sub> sources. *Atmospheric Environment*, 106, 191-195.

Fibiger, D. L., and M. G. Hastings (2016), First Measurements of the Nitrogen Isotopic Composition of NO<sub>x</sub> from Biomass Burning, *Environmental Science & Technology*, 50(21), 11569-11574, doi:10.1021/acs.est.6b03510.

Finlayson-Pitts, B. J., and J. N. Pitts, Jr. (2000), *Chemistry of the Upper and Lower Atmosphere*, Academic Press, San Diego.

Fowler, D., et al. (2013), The global nitrogen cycle in the twenty-first century, *Philosophical Transactions of the Royal Society B-Biological Sciences*, 368(1621).

Freyer, H. D. (1991). Seasonal-Variation of  $^{15}\text{N}/^{14}\text{N}$  Ratios in Atmospheric Nitrate Species. *Tellus Series B-Chemical and Physical Meteorology*, 43(1), 30-44.

Freyer, H. D., D. Kley, A. Volzthomas, and K. Kobel (1993), On the interaction of isotopic exchange processes with photochemical-reactions in atmospheric oxides of nitrogen, *Journal of Geophysical Research-Atmospheres*, 98(D8), 14791-14796, doi:10.1029/93jd00874.

Galloway, J. N., Dentener, F. J., Capone, D. G., Boyer, E. W., Howarth, R. W., Seitzinger, S. P., . & Karl, D. M. (2004). Nitrogen cycles: past, present, and future. *Biogeochemistry*, 70(2), 153-226.

Golden, D. M., and G. P. Smith (2000), Reaction of  $\text{OH} + \text{NO}_2 + \text{M}$ : A new view, *Journal of Physical Chemistry A*, 104(17), 3991-3997.

Gregory, G. L., Browell, E. V., & Warren, L. S. (1988). Boundary layer ozone: An airborne survey above the Amazon Basin. *Journal of Geophysical Research: Atmospheres*, 93(D2), 1452-1468.

Hall, J. V., A. M. Winer, M. T. Klienman, F. W. Lurmann, V. Brajer, and S. D. Colome (1992), Valuing the Health Benefits of Clean Air, *Science*, V255, 812-817.

Hastings, M. G., K. L. Casciotti, and E. M. Elliott (2013), Stable Isotopes as Tracers of Anthropogenic Nitrogen Sources, Deposition, and Impacts, *Elements*, 9(5), 339-344.

Hastings, M. G., Sigman, D. M., & Lipschultz, F. (2003). Isotopic evidence for source changes of nitrate in rain at Bermuda. *Journal of Geophysical Research: Atmospheres*, 108(D24).

Heaton, T. H. E. (1987).  $^{15}\text{N}$   $^{14}\text{N}$  ratios of nitrate and ammonium in rain at Pretoria, South Africa. *Atmospheric Environment (1967)*, 21(4), 843-852.

Hegglin, M. I., D. Brunner, T. Peter, P. Hoor, H. Fischer, J. Staehelin, M. Krebsbach, C. Schiller, U. Parchatka, and U. Weers (2006), Measurements of  $\text{NO}$ ,  $\text{NO}_y$ ,  $\text{N}_2\text{O}$ , and  $\text{O}_3$  during SPURT: implications for transport and chemistry in the lowermost stratosphere, *Atmospheric Chemistry and Physics*, 6, 1331-1350, doi:10.5194/acp-6-1331-2006.

Horowitz, L. W., J. Liang, G. M. Gardner, and D. J. Jacob (1998), Export of reactive nitrogen from North America during summertime: sensitivity to hydrocarbon chemistry, *Journal of Geophysical Research*, 103(D11), 13451-13476.

- Houlton, B. Z., Boyer, E., Finzi, A., Galloway, J., Leach, A., Liptzin, D., ... & Townsend, A. R. (2013). Intentional versus unintentional nitrogen use in the United States: trends, efficiency and implications. *Biogeochemistry*, *114*(1-3), 11-23.
- Hoyle, C. R., et al. (2011), A review of the anthropogenic influence on biogenic secondary organic aerosol, *Atmospheric Chemistry and Physics*, *11*(1), 321-343, doi:10.5194/acp-11-321-2011.
- Hudman, R. C., Moore, N. E., Mebust, A. K., Martin, R. V., Russell, A. R., Valin, L. C., & Cohen, R. C. (2012). Steps towards a mechanistic model of global soil nitric oxide emissions: implementation and space based-constraints. *Atmospheric Chemistry and Physics*, *12*(16), 7779-7795.
- Jaffe, D. A., Honrath, R. E., Zhang, L., Akimoto, H., Shimizu, A., Mukai, H., ... & Merrill, J. (1996). Measurements of NO, NO<sub>y</sub>, CO and O<sub>3</sub> and estimation of the ozone production rate at Oki Island, Japan, during PEM-West. *Journal of Geophysical Research: Atmospheres*, *101*(D1), 2037-2048.
- Kastler, J., & Ballschmiter, K. (1998). Bifunctional alkyl nitrates—trace constituents of the atmosphere. *Fresenius' journal of analytical chemistry*, *360*(7-8), 812-816.
- Kuang, C., Riipinen, I., Sihto, S. L., Kulmala, M., McCormick, A. V., & McMurry, P. H. (2010). An improved criterion for new particle formation in diverse atmospheric environments. *Atmospheric Chemistry and Physics*, *10*(17), 8469-8480.
- Lajtha, K., and J. Jones (2013), Trends in cation, nitrogen, sulfate and hydrogen ion concentrations in precipitation in the United States and Europe from 1978 to 2010: a new look at an old problem, *Biogeochemistry*, *116*(1-3), 303-334, doi:10.1007/s10533-013-9860-2.
- Lelieveld, J., et al. (2008), Atmospheric oxidation capacity sustained by a tropical forest, *Nature*, *452*(7188), 737-740.
- Lee, S. H., Uin, J., Guenther, A. B., de Gouw, J. A., Yu, F., Nadykto, A. B., ... & Baumann, K. (2016). Isoprene suppression of new particle formation: Potential mechanisms and implications. *Journal of Geophysical Research: Atmospheres*, *121*(24), 14-621.
- Lefohn, A. S., & Pinkerton, J. E. (1988). High resolution characterization of ozone data for sites located in forested areas of the United States. *JAPCA*, *38*(12), 1504-1511.
- Liang, M. C., G. A. Blake, and Y. L. Yung (2004), A semianalytic model for photo-induced isotopic fractionation in simple molecules, *Journal of Geophysical Research-Atmospheres*, *109*(D10).
- Ma, J. Z., Y. C. Liu, C. Han, Q. X. Ma, C. Liu, and H. He (2013), Review of heterogeneous photochemical reactions of NO<sub>y</sub> on aerosol - A possible daytime source of nitrous acid (HONO) in the atmosphere, *Journal of Environmental Sciences-China*, *25*(2), 326-334, doi:10.1016/s1001-0742(12)60093-x.



- Madronich, S. (1987). Photodissociation in the atmosphere: 1. Actinic flux and the effects of ground reflections and clouds. *Journal of Geophysical Research: Atmospheres*, 92(D8), 9740-9752.
- McMurry, P. H., Fink, M., Sakurai, H., Stolzenburg, M. R., Mauldin III, R. L., Smith, J., ... & Huey, L. G. (2005). A criterion for new particle formation in the sulfur-rich Atlanta atmosphere. *Journal of Geophysical Research: Atmospheres*, 110(D22).
- Michalski, G., R. Jost, D. Sugny, M. Joyeux, and M. Thiemens (2004), Dissociation energies of six NO<sub>2</sub> isotopologues by laser induced fluorescence and zero point energy of some triatomic molecules *Journal of Chemical Physics*, 121(15), 7153-7161.
- Miller, C. E., and Y. L. Yung (2000), Photo-induced isotopic fractionation, *Journal of Geophysical Research-Atmospheres*, 105(D23), 29039-29051.
- Monks, P.S. (2005) Gas-phase radical chemistry in the troposphere. *Chemical Society Reviews*. 2005 DOI: 10.1039/b307982c
- Morino, Y., Y. Kondo, N. Takegawa, Y. Miyazaki, K. Kita, Y. Komazaki, M. Fukuda, T. Miyakawa, N. Moteki, and D. R. Worsnop (2006), Partitioning of HNO<sub>3</sub> and particulate nitrate over Tokyo: Effect of vertical mixing, *Journal of Geophysical Research-Atmospheres*, 111(D15), doi:10.1029/2005jd006887.
- Moore, H. (1977). The isotopic composition of ammonia, nitrogen dioxide and nitrate in the atmosphere. *Atmospheric Environment (1967)*, 11(12), 1239-1243.
- Pan, Y. P., S. L. Tian, D. W. Liu, Y. T. Fang, X. Y. Zhu, M. Gao, G. R. Wentworth, G. Michalski, X. J. Huang, and Y. S. Wang (2018), Source Apportionment of Aerosol Ammonium in an Ammonia-Rich Atmosphere: An Isotopic Study of Summer Clean and Hazy Days in Urban Beijing, *Journal of Geophysical Research-Atmospheres*, 123(10), 5681-5689, doi:10.1029/2017jd028095.
- Paulot, F., P. Ginoux, W. F. Cooke, L. J. Donner, S. Fan, M. Y. Lin, J. Mao, V. Naik, and L. W. Horowitz (2016), Sensitivity of nitrate aerosols to ammonia emissions and to nitrate chemistry: implications for present and future nitrate optical depth, *Atmospheric Chemistry and Physics*, 16(3), 1459-1477, doi:10.5194/acp-16-1459-2016.
- Petäjä, T., Mauldin Iii, R. L., Kosciuch, E., McGrath, J., Nieminen, T., Paasonen, P., ... & Kulmala, M. (2009). Sulfuric acid and OH concentrations in a boreal forest site. *Atmospheric Chemistry and Physics*, 9(19), 7435-7448.
- Pilegaard, K. (2013). Processes regulating nitric oxide emissions from soils. *Phil. Trans. R. Soc. B*, 368(1621), 20130126
- Platt, U. F., A. M. Winer, H. W. Biermann, R. Atkinson, and J. N. Pitts (1984), Measurement of Nitrate Radical Concentrations in Continental Air, *Environmental Science & Technology*, 18(5), 365-369.

- Prinn, R. G. (2003), The cleansing capacity of the atmosphere, *Annual Review of Environment and Resources*, 28, 29-57.
- Pusede, S. E., et al. (2016), On the effectiveness of nitrogen oxide reductions as a control over ammonium nitrate aerosol, *Atmospheric Chemistry and Physics*, 16(4), 2575-2596, doi:10.5194/acp-16-2575-2016.
- Pye, H. O. T., A. W. H. Chan, M. P. Barkley, and J. H. Seinfeld (2010), Global modeling of organic aerosol: the importance of reactive nitrogen (NO<sub>x</sub> and NO<sub>3</sub>), *Atmospheric Chemistry and Physics*, 10(22), 11261-11276.
- Qi, X. M., Ding, A. J., Nie, W., Petäjä, T., Kerminen, V. M., Herrmann, E., and Sun, J. N. (2015). Aerosol size distribution and new particle formation in the western Yangtze River Delta of China: 2 years of measurements at the SORPES station. *Atmospheric chemistry and physics*, 15(21), 12445-12464.
- Richet, P., Y. Bottinga, and M. Javoy (1977), Review of hydrogen, carbon, nitrogen, oxygen, sulfur, and chlorine stable isotope fractionation among gaseous molecules, *Annual Review of Earth and Planetary Sciences*, 5, 65-110
- Riemer, N., Vogel, H., Vogel, B., Anttila, T., Kiendler-Scharr, A., and Mentel, T. F. (2009). Relative importance of organic coatings for the heterogeneous hydrolysis of N<sub>2</sub>O<sub>5</sub> during summer in Europe. *Journal of Geophysical Research: Atmospheres*, 114(D17).
- Riemer, N., H. Vogel, B. Vogel, B. Schell, I. Ackermann, C. Kessler, and H. Hass (2003), Impact of the heterogeneous hydrolysis of N<sub>2</sub>O<sub>5</sub> on chemistry and nitrate aerosol formation in the lower troposphere under photo-smog conditions, *Journal of Geophysical Research*, 108(D4), 4144-DOI: 4110.1029/2002JD002436.
- Riha, K. M. (2013). The use of stable isotopes to constrain the nitrogen cycle. Purdue University, West Lafayette, IN
- Roehl, C. M., J. J. Orlando, G. S. Tyndall, R. E. Shetter, G. J. Vazquez, C. A. Cantrell, and J. G. Calvert (1994), Temperature-dependence of the quantum yields for the photolysis of NO<sub>2</sub> near the dissociation limit, *Journal of Physical Chemistry*, 98(32), 7837-7843, doi:10.1021/j100083a015.
- Romer, P. S., Duffey, K. C., Wooldridge, P. J., Allen, H. M., Ayres, B. R., Brown, S. S., ... & Feiner, P. A. (2016). The lifetime of nitrogen oxides in an isoprene-dominated forest. *Atmospheric Chemistry and Physics*, 16(12), 7623-7637.
- Rose, L. A., Yu, Z. J., Bain, D. J., & Elliott, E. M. (2019). High resolution, extreme isotopic variability of precipitation nitrate. *Atmospheric Environment*, 207, 63-74. 10.1016/j.atmosenv.2019.03.012

Savard, M. M., Cole, A., Smirnoff, A., & Vet, R. (2017).  $\delta^{15}\text{N}$  values of atmospheric N species simultaneously collected using sector-based samplers distant from sources—Isotopic inheritance and fractionation. *Atmospheric environment*, 162, 11-22.

Sharma, H. D., R. E. Jervis, and K. Y. Wong (1970), Isotopic exchange reactions in nitrogen oxides, *Journal of Physical Chemistry*, 74(4), 923-933.

Shepherd, M. F., Barzetti, S., & Hastie, D. R. (1991). The Production of Atmospheric  $\text{NO}_2$  and  $\text{N}_2\text{O}$  from a Fertilized Agricultural Soil.

Shrivastava, M., Cappa, C. D., Fan, J., Goldstein, A. H., Guenther, A. B., Jimenez, J. L., ... & Petaja, T. (2017). Recent advances in understanding secondary organic aerosol: Implications for global climate forcing. *Reviews of Geophysics*, 55(2), 509-559.

Snyder, J. A., D. Hanway, J. Mendez, A. J. Jamka, and F. M. Tao (1999), A density functional theory study of the gas-phase hydrolysis of dinitrogen pentoxide, *Journal of Physical Chemistry A*, 103(46), 9355-9358.

Spak, S. N., and T. Holloway (2009), Seasonality of speciated aerosol transport over the Great Lakes region, *Journal of Geophysical Research-Atmospheres*, 114.

Srivastava, R. K., Neuffer, W., Grano, D., Khan, S., Staudt, J. E., & Jozewicz, W. (2005). Controlling  $\text{NO}_x$  emission from industrial sources. *Environmental progress*, 24(2), 181-197.

Seinfeld, J. H., and S. N. Pandis (1998), *Atmospheric chemistry and physics : from air pollution to climate change*, 1 ed., New York : Wiley.

Stockwell, W. R., F. Kirchner, M. Kuhn, and S. Seefeld (1997), A new mechanism for regional atmospheric chemistry modeling, *Journal of Geophysical Research*, 102(D22), 25847-25879.

Stockwell, W. R., P. Middleton, J. S. Chang, and X. Y. Tang (1990), The 2nd Generation Regional Acid Deposition Model Chemical Mechanism for Regional Air-Quality Modeling, *Journal of Geophysical Research-Atmospheres*, 95(D10), 16343-16367.

Urey, H. C. (1947), Thermodynamic properties of isotopic substances, *J. Chem. Soc*, 562-581.

Van Hook, W. A., L. P. N. Rebelo, and M. Wolfsberg (2001), An interpretation of the vapor phase second virial coefficient isotope effect: Correlation of virial coefficient and vapor pressure isotope effects, *Journal of Physical Chemistry A*, 105(40), 9284-9297, doi:10.1021/jp004305z.

Vandaele, A. C., C. Hermans, S. Fally, M. Carleer, R. Colin, M. F. Merienne, A. Jenouvrier, and B. Coquart (2002), High-resolution Fourier transform measurement of the  $\text{NO}_2$  visible and near-infrared absorption cross sections: Temperature and pressure effects, *Journal of Geophysical Research-Atmospheres*, 107(D18), doi:10.1029/2001jd000971.

Walters, W., S. Goodwin, Michalski, and G. (2015a), Nitrogen Stable Isotope Composition of Vehicle Emitted  $\text{NO}_x$ , *Environmental Science and Technology*, 49(4), 2278-2285.

Walters, W. W., H. Fang, and G. Michalski (2018), Summertime diurnal variations in the isotopic composition of atmospheric nitrogen dioxide at a small midwestern United States city, *Atmospheric Environment*, 179, 1-11, doi:10.1016/j.atmosenv.2018.01.047.

Walters, W. W., and G. Michalski (2015), Theoretical calculation of nitrogen isotope equilibrium exchange fractionation factors for various NO<sub>y</sub> molecules, *Geochimica Et Cosmochimica Acta*, 164, 284-297, doi:10.1016/j.gca.2015.05.029.

Walters, W. W., and G. Michalski (2016), Ab initio study of nitrogen and position-specific oxygen kinetic isotope effects in the NO + O<sub>3</sub> reaction, *Journal of Chemical Physics*, 145(22), doi:10.1063/1.4968562.

Walters, W. W., D. S. Simonini, and G. Michalski (2016), Nitrogen isotope exchange between NO and NO<sub>2</sub> and its implications for <sup>15</sup>N variations in tropospheric NO<sub>x</sub> and atmospheric nitrate, *Geophysical Research Letters*, 43(1), 440-448, doi:10.1002/2015gl066438.

Walters, W. W., B. D. Tharp, H. Fang, B. J. Kozak, and G. Michalski (2015b), Nitrogen Isotope Composition of Thermally Produced NO<sub>x</sub> from Various Fossil-Fuel Combustion Sources, *Environmental Science & Technology*, 49(19), 11363-11371, doi:10.1021/acs.est.5b02769.

Wolfsberg, M. (1960), Note on secondary isotope effects in reaction rates, *Journal of Chemical Physics*, 33(1), 2-6, doi:10.1063/1.1731078.

Wolfsberg, M., W. A. Van Hook, P. Paneth, L. P. N. Rebelo, M. Wolfsberg, W. A. VanHook, and P. Paneth (2010), *Isotope Effects on Equilibrium Constants of Chemical Reactions; Transition State Theory of Isotope Effects*, 77-137 pp., doi:10.1007/978-90-481-2265-3\_4.

Yu, Z., & Elliott, E. M. (2017). Novel method for nitrogen isotopic analysis of soil-emitted nitric oxide. *Environmental Science & Technology*, 51(11), 6268-6278.

Zhang, Y., K. Vijayaraghavan, X. Y. Wen, H. E. Snell, and M. Z. Jacobson (2009), Probing into regional ozone and particulate matter pollution in the United States: 1. A 1 year CMAQ simulation and evaluation using surface and satellite data, *Journal of Geophysical Research-Atmospheres*, 114.